

## Review

## Nanoscale thermoplasmonic welding

Lin Wang,<sup>1</sup> Yijun Feng,<sup>1</sup> Ze Li,<sup>1</sup> and Guohua Liu<sup>1,\*</sup>

## SUMMARY

**Establishing direct, close contact between individual nano-objects is crucial to fabricating hierarchical and multifunctional nanostructures. Nanowelding is a technical prerequisite for successfully manufacturing such structures. In this paper, we review the nanoscale thermoplasmonic welding with a focus on its physical mechanisms, key influencing factor, and emerging applications. The basic mechanisms are firstly described from the photothermal conversion to self-limited heating physics. Key aspects related to the welding process including material scrutinization, nanoparticle geometric and spatial configuration, heating scheme and performance characterization are then discussed in terms of the distinctive properties of plasmonic welding. Based on the characteristics of high precision and flexible platform of thermoplasmonic welding, the potential applications are further highlighted from electronics and optics to additive manufacturing. Finally, the future challenges and prospects are outlined for future prospects of this dynamic field. This work summarizes these innovative concepts and works on thermoplasmonic welding, which is significant to establish a common link between nanoscale welding and additive manufacturing communities.**

## INTRODUCTION

The development of miniaturization, intelligence, and functional devices inspires people to explore ways to break through the size limit of devices. The current manufacturing technology has achieved a state-of-the-art precision to the nanoscale (Baljon and Robbins, 1996; Patolsky et al., 2004). Nanoscale welding is an emerging field to promote the connection of individual nano-objects, providing high mechanical strength of bonds between different structural elements with excellent electrical and optical connectivity (Zhou, 2008). Nanoscale welding can be classified into three types in terms of the physical states of joint: solid-state bonding, brazing, and fusion welding (Krzanowski, 1989; Lin et al., 2015; Peng et al., 2017; Shehla et al., 2016). Solid-state cold welding achieves the bonding through atomic diffusion (Dai et al., 2016; Liu et al., 2017; Wagle and Baker, 2015). This method requires the weld surface free of impurities with a high surface energy (Changsoon Kim et al., 2000; Chen et al., 2012a; Lu et al., 2010). The high surface energy of nanomaterials is often used as brazing filler to connect other materials, retaining the integrity of the connected objects and respective structures and functions (Gao and Gu, 2010; Gu et al., 2005). Whereas the obvious disadvantages lie in only one joint being formed at a time, and the operation requires a precise management of the nanoscale components (Peng et al., 2009). The heat supply is critically important to creating high-quality joints in nanoscale welding, as the high specific surface energy and increased surface volume ratio of materials are very sensitive to heat (Wagle and Baker, 2015). For example, fusion welding, such as Joule heating (Chellattoan et al., 2019; Song et al., 2014; Tohmyoh et al., 2007), electron beam welding (Koleva, 2005; Terrones et al., 2002; Zhang et al., 2018), and ultrafast laser welding (Gonzalez-Rubio et al., 2017; Huang et al., 2012; Itoh et al., 2013), have been applied for nano-connection, but these methods with high energy input unavoidably damage finer nano-objects. Therefore, it is highly necessary to develop accurate welding technology to solve these issues.

Plasmon-assisted welding process configures an emerging field-thermoplasmonic welding, in which light absorption and heat generation are the competitive mechanisms to tune the temperature distribution of metal structures. In this way, metal nanoparticles are used as nano-heat sources during light illumination for a self-limited bonding that meets the requirements of high precision, low energy input, and large-scale application (Hartland, 2011). Light-matter interaction via nano-gaps of materials results in significant enhancement of the electromagnetic field, which concentrates heat at the desired point where the

<sup>1</sup>Beijing Key Laboratory of Multiphase Flow and Heat Transfer for Low Grade Energy Utilization, North China Electric Power University, Beijing 102206, China

\*Correspondence: liuguohua126@126.com  
<https://doi.org/10.1016/j.isci.2022.104422>



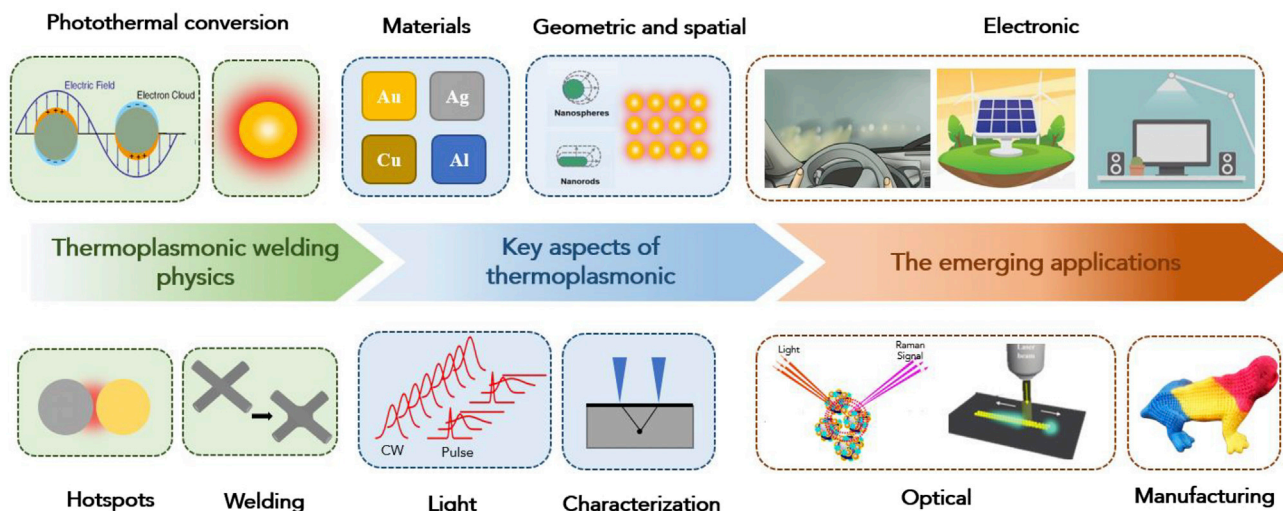


**Figure 1. Schematic of the structure of this article**

Overview of thermoplasmonic welding from its physics and key factors to the emerging applications. Reprinted and adapted with permission from references (Ha et al., 2019; Hardiansyah et al., 2015; Powell et al., 2018; Sevenler et al., 2015; Su et al., 2013). Copyright 2015, Springer Japan. Copyright 2019, American Chemical Society. Copyright 2013, WILEY-VCH. Copyright 2015, Springer Verlag. Copyright 2018, American Chemical Society.

materials to be bonded together. The geometry-dependent heating of junction causes the welding process to be self-limited when a physical connection is made. This self-limited process can prevent damage to low-thermal-budget substrates (Park et al., 2016). The light source is used to excite the heating for achieving the fine-tuned and start-stop of welding (Jauffred et al., 2019). Especially when using a pulsed laser, thermoplasmonic quickly adjusts the temperature of nanostructures with unprecedented time and spatial control (Garnett et al., 2012). The light-induced nano-welding has the advantage of non-contact, high operational efficiency, and compatibility with flexible manufacturing systems. It has been used to connect zero dimension nanoparticles (NPs), one dimension nanowire (NW), and two-dimensional materials (Lee et al., 2016; Pan et al., 2007; Rahimi et al., 2016). Specifically, NPs can be facile welded into NP chains or thin films (Mafune et al., 2003). NWs are usually welded for electrical connection in conductive electrodes (Kim et al., 2013). Furthermore, thermoplasmonic welding has been integrated with other technologies such as roll-to-roll and inkjet printing processes for large-scale production (Ko et al., 2007; Nian et al., 2015).

Thermoplasmonic welding has been used to robustly bond nano-components to create novel mechanical and electrical properties owing to its tunable optical and plasmonic properties, but there is still a lack of systematic knowledge on this emerging technology. Herein, we review the research status of thermoplasmonic welding, from its physics and key factors to the potential applications (Figure 1). First, we discuss the physical mechanism of thermoplasmonic welding that includes the photothermal conversion and self-limited heating. Key aspects of thermoplasmonic welding such as optical, photothermal, electrical, and mechanical, the material scrutinization, geometric and spatial configuration, heat scheme as well as performance characterization, are then emphasized. Moreover, the potential applications of this technology are highlighted from an electrical device, optical application to additive manufacturing. Finally, we provide our views on future research directions in thermoplasmonic welding, together with a few suggestions for further developments of this technology.

## THERMOPLASMONIC WELDING PHYSICS

Thermoplasmonic welding is achieved via two sequential steps: photothermal conversion and self-limited welding. The discussion of photothermal conversion includes the introduction of the light-matter interaction and light concentration before proceeding to the most crucial heating effect. Moreover, the self-limited welding is detailed by thermal localization and melting-solidification of the materials.

### Photothermal conversion

#### Light-matter interaction

Nanostructures illuminated by light lead to a local surface plasmon resonance (LSPR) that oscillates around the structure with a distinct frequency (Figure 2A) (Sevenler et al., 2015; Willets and Van Duyne, 2007).

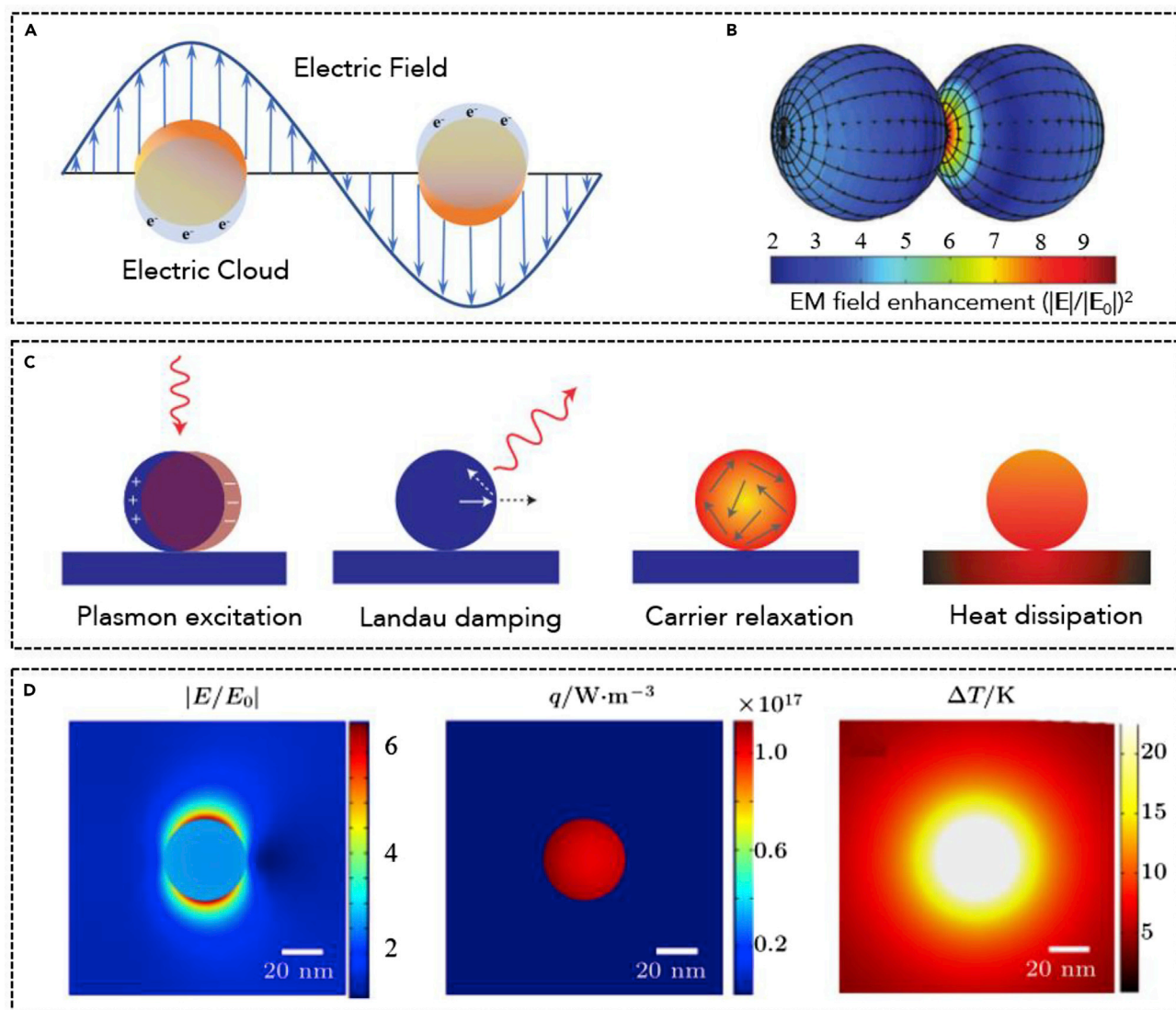


**Figure 2. Photothermal conversion of plasmonic materials**

(A) Schematic of LSPR. Reprinted and adapted with permission from Willets and Van Duyne (2007). Copyright 2007, Annual Reviews Inc.

(B) Field strength distribution of external hotspot model. Reprinted and adapted with permission from Le Ru and Etchegoin (2012). Copyright 2018, Elsevier Ltd.

(C) Photoexcitation and relaxation of plasmonic NPs. Reprinted and adapted with permission from Brongersma et al. (2015). Macmillan Publishers Limited. Copyright 2015, Macmillan Publishers Limited.

(D) Electromagnetic, thermal density, and temperature field distribution of Au NP. Reprinted and adapted with permission from Chen et al. (2012b). Copyright 2012, American Chemical Society.

The prerequisite of this depends on the characteristic frequency of oscillation consistent with that of the excitation frequency of light (Baffou and Quidant, 2014). The electromagnetic (EM) field interacts with electrons, which causes them beyond equilibrium, generating surface charge on the nanostructure. The system tends to relax to its minimum-energy configuration with the electrons returning to the equilibrium status, inducing charge-density oscillations (Giannini et al., 2010). LSPRs can squeeze light into nanometer dimensions, allowing the manipulation of light and heat at the nanoscale (Taminiau et al., 2008). The interaction between light and nanostructure is described by the classical Maxwell's equations, and the electric field distribution can be calculated from the Helmholtz wave equation (Cunha et al., 2020):

$$\nabla \times u_r^{-1}(\nabla \times \mathbf{E}) - \left(\frac{\omega}{c_0}\right)^2 \epsilon_m \mathbf{E} = 0 \quad (\text{Equation 1})$$

Here, we suppose that  $|\mathbf{E}| \propto \exp(-i\omega t)$ ,  $\omega$  is the angular frequency of incident light,  $\mu_r$  is the magnetic permeability,  $\epsilon_m$  is the permittivity of the surrounding medium, and  $\epsilon$  is the permittivity of materials. Subsequently, the metal structure acts on part of the energy carried by incident light, dissipating it in the form of heat within NP or reradiating it again into free space, which corresponds to the concepts of absorption and scattering, respectively (Baffou and Quidant, 2014).

### Light concentration

The plasmonic coupling between adjacent particles concentrates the light into highly localized regions and increases the EM field in the narrow gap (a factor of up to  $10^6$ ). Such regions of intense fields are referred to as hotspots (Figure 2B) (Le Ru and Etchegoin, 2012). These hotspots show multiple resonances, and the wavelength of characteristic dipole resonance is wider than that of single NP. Hotspots enable the effective light concentration limited to the nanoscale gap through plasmon excitation, producing the intense EM field at the point (Garnett et al., 2012). The EM field generated by concentrated gap can be expressed by Equation (Eom, 2004):

$$\mathbf{E} = \mathbf{E}_0 \frac{\epsilon_1 - \epsilon \alpha^2}{\epsilon_1 + \epsilon \rho^2} \quad (\text{Equation 2})$$

where  $\mathbf{E}$  is the electric field,  $\mathbf{E}_0$  is the electric field of the incident light,  $\epsilon_1$  is the frequency-dependent permittivity of air,  $\alpha$  is the NP radius, and  $\rho$  is the distance from the NP center. The hotspots are generated between various nanostructures with the nanoscale gap (1–10 nm), such as NWs, nanoclusters, and NP aggregation films (Halas et al., 2011; Salmon et al., 2020). It is worth mentioning that the tip of a single nano-object also produces hotspots, but their heat source density does not fully match these hotspots. This is because the hotspot usually comes from the tip and charge accumulation at the metal interface, whereas the heat comes from the area where the charge flows freely (Ma et al., 2014).

### Heat generation

After the NPs absorb the energy of the incident light, the free electrons in the surface resonate on the lattice, and are then excited to reach a higher energy level at the Fermi level, leading to a charge distribution (Brongersma et al., 2015). Plasmon resonances in nanostructures are damped radiatively by re-emission of photons or non-radiatively through electron-hole pairs via Landau damping. These electrons jump to the excited state that exhibits a non-equilibrium energy distribution, redistributing their thermal energy by electron-electron scattering (Figure 2C) (Chen et al., 2019a; Wang et al., 2021). The subsequent phonon-coupling process refers to the accumulation of energy in the crystal lattice, leading to the heating of particles (Liu et al., 2020). The light-to-heat conversion depends on the local electric field enhancement and light absorption controlled by the relaxation process of surface plasmons at different time scales. The generated heat  $Q_{\text{abs}}$  is directly related to the imaginary part of the dielectric constant of material (Chen et al., 2012b):

$$Q_{\text{abs}} = \frac{\omega}{2} \epsilon_0 \text{Im}\{\epsilon\} |\mathbf{E}|^2 \quad (\text{Equation 3})$$

where  $\epsilon_0$  is the permittivity of vacuum;  $\omega$  is the angular frequency of light. When the structure scale is far smaller than the wavelength, the electric field inside the NP is approximately uniform, and the resulting heat flux is relatively uniform (Liu et al., 2001). as the thermal conductivity of metal NP is far greater than that of the surrounding medium, the heat energy generated inside the particle would diffuse in a very short time, so the nanostructure temperature is considered uniform (Figure 2D) (Chen et al., 2012b). The existence of hotspots between adjacent materials increases the heat generation in a gap region where the temperature is higher than that of the other surrounding regions. Therefore, hotspot heating leads to non-uniform temperature distribution over the materials, which is conducive to the subsequent self-limited welding.

### Self-limited welding

#### The melting processes

Thermoplasmonic welding involves the melting and solidification of nanomaterials. Owing to the increased surface energy, the melting temperature of NPs is much lower than that of bulk metals (Van Teijlingen et al.,

2020). The melting point of size-dependent nanomaterials can be calculated through the classical thermodynamic analysis Gibbs–Thomson equation (Van Teijlingen et al., 2020):

$$T_M(d) = T_{MB} \left( 1 - \frac{4\sigma_{sl}}{H_f \rho_s d} \right) \quad (\text{Equation 4})$$

$T_{MB}$  is the bulk melting point;  $\sigma_{sl}$  is solid-liquid interface energy;  $H_f$  is the bulk heat of fusion;  $\rho_s$  density of solid and  $d$  is NP's diameter. There is a decrease in the melting point with a decrease in the particle size. For example, the melting temperature (300–500°C) of Au nanostructure is much lower than the melting point of bulk gold (1,064°C) (Karim et al., 2006). Once the gap temperature is higher than the melting point, the phase transition is initiated at the NP surface. With the continuous melting of surface lattice, the metal neck composed of many individual NPs would gradually be formed. If heterogeneous NPs are welded, the material with a lower melting point is heated and melted into liquid as nano-solder to realize the connection of other materials. The intensity of hotspots determines the melting process and final aggregation of these NPs.

### The solidification processes

The material solidification includes nucleation, growth, and recrystallization. The thermodynamic physics of crystal nuclei is the reduction of free energy caused by undercooling, and the kinetic physics is the degree of reduction of free energy (Bauerle, 2011). After nucleation, the lattice gradually grows, whereas the temperature remains unchanged, the microstructure begins to coarsen and starts to produce new internal stress (Chen et al., 2011). When the welding materials are in contact with each other and have the same crystal structure, the epitaxially regrow of metals from existing materials does not require nucleation. In this case, as long as the temperature drops below the liquidus, spontaneous growth can be realized without an activation energy barrier (DebRoy et al., 2018).

The crystallization process is controlled by temperature gradient and crystal growth rate that determine the solidification mode and the size of the crystal structure (Figure 3). The microstructure in the fusion zone features different morphologies, such as planar, cellular, and dendritic, which are tuned by a temperature gradient, grain growth rate, and undercooling (Kou, 2003). With increasing undercooling, the microstructure shifts from planar to cellular and from cellular to dendritic or exhibits a combination of these. Because the base material is much colder than molten metal, the first grains solidify as dendrites. In this process, relative to crystal growth, the thermal gradient is dominant. After some time, the supercooling effect decreases, and solidification tends to be planar, and the secondary grain grows, forming epitaxial recrystallization. The secondary growth enlarges some grains at the expense of other grains. With increasing interface free energy, lattice-matched substrates help drive epitaxial recrystallization. The solidification of grains tends to be planar epitaxial growth mode. In the process of competitive grain growth, new grains form on the original grains and grow along the denser crystallographic direction perpendicular to the isotherm (Oliveira et al., 2020). Owing to the increase of interfacial free energy, lattice-matched substrates can drive epitaxial recrystallization, depending on factors such as temperature, pressure, monography, self-diffusion, and environment. In thermoplasmonic welding, the atoms in the bottom nanomaterials must have migration, allowing epitaxial recrystallization at the junction. The self-limited heating characteristics of welding is mainly involved in the solidification stage. When the adjacent nanostructures begin to weld together, the generated heat moves from the original gap to the joint. Therefore, a zipper effect is produced, and the heat generation always reaches its peak at the edge of the gap and moves outward. Once the materials are physically connected, the plasmon mode in the junction is no longer excited, and thus the heat generation is reduced. With the progress of welding, the generated heat decreases rapidly until the hotspots are disappeared in nanogaps (Garnett et al., 2012). This self-limited feature improves material stability because it prevents the nanomaterials from breaking up during intensive heating. Thermal, electrical, and physical properties of the joint would more closely resemble the properties of bulk material (Yang et al., 2013).

## KEY ASPECTS OF THERMOPLASMONIC WELDING

This section discusses key aspects of the thermoplasmonic welding including material scrutinization, NPs' geometric and spatial configuration, heating scheme, and the performance characterization.

### Material scrutinization

Nature material properties affect the welding process, such as optical performance, melting point, and stability. From the optical point of view, plasmonic metals have the intrinsic properties of plasmon resonance.

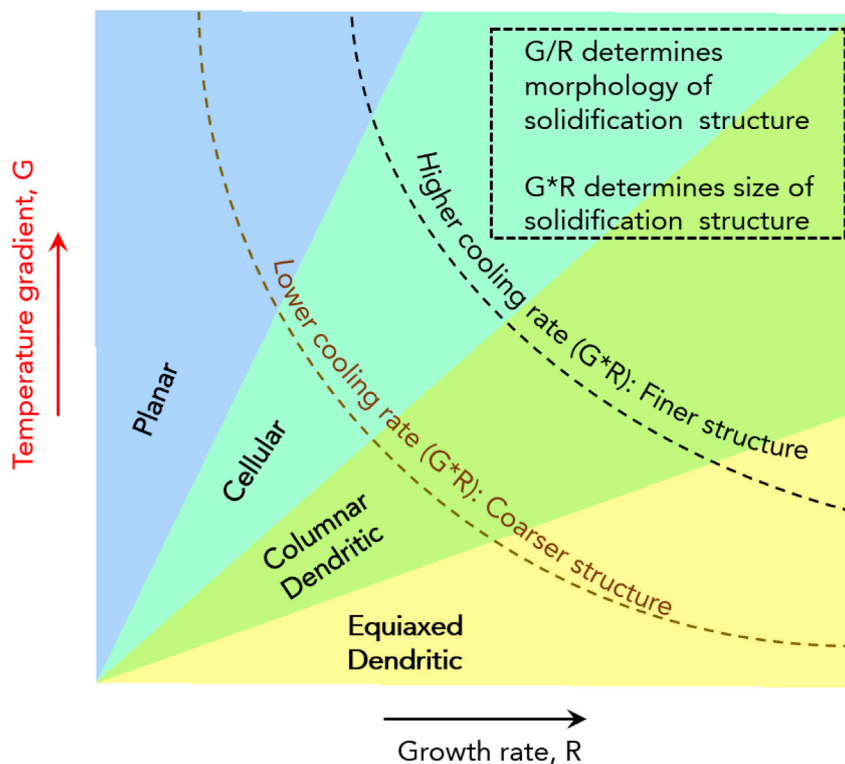


**Figure 3. Schematic representation of the solidification microstructures**

The effect of temperature gradient and growth rate on the solidification structures. Reprinted and adapted with permission from [DeRoy et al. \(2018\)](#). Copyright 2017, Elsevier Ltd.

For example, Al and Pd NPs are plasmonic active in the UV range, whereas Ag, Au, and Cu NPs mainly work in the wavelength range of 400–650 nm related to their permittivity ([Chen et al., 2013](#); [Eustis and el-Sayed, 2006](#); [Park et al., 2012](#); [Wei and Eilers, 2009](#)). Al, Mg, and Ga are functional in the UV region owing to the high frequency of plasmon. To quantify the thermoplasmonic performance, the dimensionless parameters are defined to highlight the advantages of different plasmonic materials, including Faraday number  $Fa$  and Joule number  $Jo$  ([Lalisse et al., 2015](#)). The  $Fa$  number is defined for quantifying the ability of a nanoparticle to enhance the electric field intensity in its surrounding medium. The  $Jo$  number enables the comparison in different environments at a fixed light irradiance, and not at a fixed incoming electric field amplitude. [Figure 4](#) shows the calculation results of the Faraday number and Joule number of some metals, in which the resonance intensity of Ag NP is the highest, which is beneficial to the application of resonance excitation, followed by Au NP, and then Cu NP. In addition, Al is also considered an ideal choice in some cases with its excellent plasmon properties in the UV range ([Knight et al., 2012](#); [Lecarme et al., 2014](#)).

Melting point is one of the key parameters to be concerned with during the welding process. Materials with different melting points need to scrutinize suitable illumination schemes toward a better welding. The use of materials with high melting points implies more energy should be input into the nanogap. The refractory metals, such as tungsten (W), molybdenum (Mo), or metal nitride, have high melting points and that can sustain high temperature (TiN 2,930°C, ZrN 2,952°C). But these materials are difficult to meet the low-temperature welding process. It is thus suitable for welding with low thermal sensitivity and no phase change requirements. At the same time, low melting point materials need to pay attention to the fragmentation of NPs. Some studies have proved that when these materials reach the optical breakdown temperature, the nanoparticles will be broken ([Pustovalov et al., 2008](#)).

The stability of the joint is important to assess the welding performance. The metal is degraded after a long-term exposing to air/oxygen or humidity, causing problems such as oxidation and optical loss ([Chan et al., 2007](#)). For example, after 36 h of contact with air, Ag NPs measured a shift of the resonance wavelength of 65 nm, attributed to sulfur contamination and the formation of  $Ag_2S$  on the NP surface

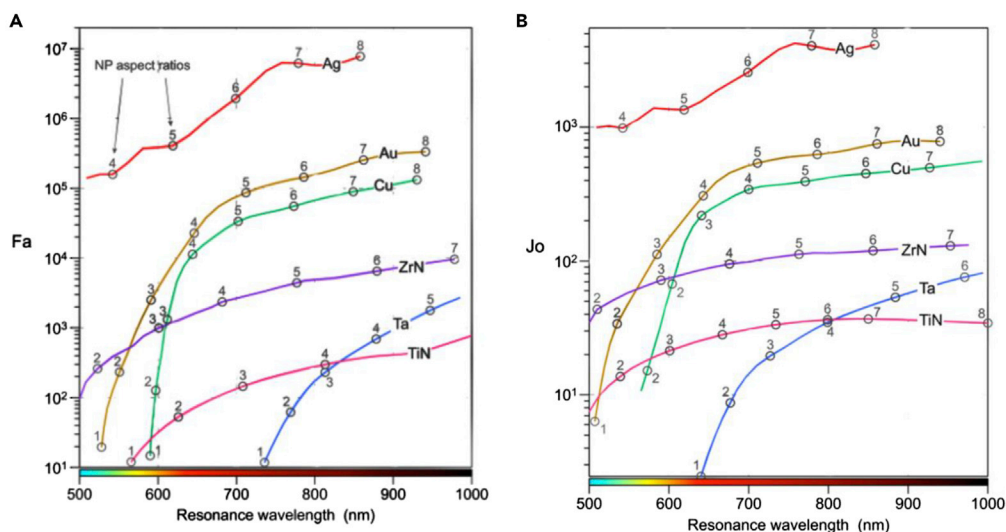


**Figure 4. Dimensionless numbers of the Faraday number and Joule number**

(A) Faraday numbers  $F_a$  at the plasmon resonance.

(B) Joule numbers  $J_o$  at the plasmon resonance. Reprinted and adapted with permission from Lalissee et al. (2015).

Copyright 2015, American Chemical Society.

(McMahon et al., 2005). In these circumstances, Ag NPs even features a lower scattering yield than Au NPs. Al suffers from the same problem as Ag and oxidizes even more rapidly (Sanz et al., 2013). But, the oxide layer  $Al_2O_3$  makes the plasmon resonance sharper (Sobhani et al., 2015). The oxidation rate of Cu is lower than that of Ag and Al, but the oxidation of Cu NPs cannot be ignored during welding. Compared with the bulk matter, the oxidation rate of nanomaterials accelerates with an increase in the surface area, which hinders the development of manufacturing technology. Many experiments are carried out in a vacuum to prevent oxidation issues. AuNPs are not easy to oxidize in the air and remain chemically stable in many environments, and it is one of the most popular materials in thermoplasmonic applications (McMahon et al., 2013).

### Geometric and spatial configuration

Particle geometry is the key factor for light absorption (Giannini et al., 2010). Adjustment of NP size tune the position and width of LSPR (Kreibig and Vollmer, 1995). When the plasmon wavelength is larger than the incident light wavelength, the electromagnetic interaction between long-distance charges inside the particles leads to the redshift (Murray and Barnes, 2007). Particles smaller than the wavelength of light (<25 nm) show effective absorption at the resonance wavelength, highlighting their advantages in converting light into heat (Chen et al., 2021; Jiang et al., 2013). Tuning particle shape has a more intense effect on LSPR (Figure 5A) (Ha et al., 2019; Ross et al., 2014). For anisotropic metal NPs, electrons oscillate to different amplitudes along the three axes of the nano-object (Reguera et al., 2017). These different oscillations in splitting the plasmon band into two or more bands (Reguera et al., 2017). By progressively increasing the aspect ratio of nanorods with a fixed diameter, the extinction cross-sections of both the longitudinal and transverse plasmon modes are enlarged (Chen et al., 2013). By customizing their aspect ratio, longitudinal mode plasmon wavelength can be tuned to cover the visible and near-infrared regions (Chen et al., 2010).

Plasmon-coupling over multiple particles creates a strong photothermal effect. The NP configuration offers another degree of freedom in tuning their optical and electric properties (Klinkova et al., 2014). Plasmonic properties can be tailored by changing the number of NPs and fine-tuning interparticle distance. When individual particles are coupled with each other, the surface plasmon resonance changes dramatically (Liu and Xue, 2021). The EM coupling of multiple NPs becomes effective when the gap distances are five times less than the radius (Quinten and Kreibig, 1986). The plasmon-coupling modes lead to the redshift and broadening of longitudinal plasmon resonance. Meanwhile, the existence of many mobile electrons strengthens the thermal effect, especially when the plasmon resonance or optical frequency approaches to the collective resonance. Two mechanisms of interaction are related to the heating process: cumulative

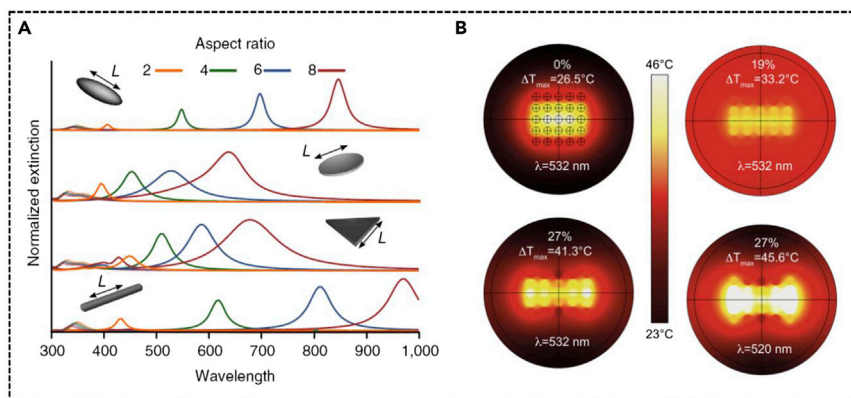


**Figure 5. Impact of geometry and spatial morphology on thermoplasmonics**

(A) Spectrum of particles with a diverse shape. Reprinted and adapted with permission from Ross et al. (2014). Copyright 2014, Macmillan Publishers Limited.

(B) Thermal maps of the multiple nanoparticles in different stretching percentages and wavelengths. Reprinted and adapted with permission from Emanuele Lio et al. (2020). Copyright 2020, AIP Publishing.

effect and Coulomb interaction (Govorov and Richardson, 2007). The cumulative effect comes from the superposition of heat flux generated by individual NPs. Under the influence of this effect, increasing the number of NPs is conducive to improving the temperature rise in the system (Baffou et al., 2010). The heating effect may come from the plasmon resonance displacement caused by the Coulomb interaction between particles, depending on the gap distance and arrangement of particles (Richardson et al., 2006). For example, that modify the arrangements through an externally applied strain could change the wavelength corresponding to the plasmonic resonance of the initial system, thereby affecting the increase in the temperature (Figure 5B) (Emanuele Lio et al., 2020). Reducing the distance between NPs lead to a strong interaction between particles (Govorov and Richardson, 2007). At present, some studies have made it possible for high-density hybrid LSPR to enhance light absorption and improve the heating temperature by randomly distributing NPs in pores (Zhou et al., 2016a, 2017).

### Heating scheme

Heat is the key parameter in thermoplasmonic welding that can be run with different schemes. Using different light sources results in different welding temperatures (Deng et al., 2019; Lee et al., 2018; Zhou et al., 2016b). Here we discuss the difference between continuous wave (CW) and pulsed irradiation. CW irradiation is the method of continuous heating, providing thermal energy distribution along the structure. Therefore, it is suitable for large processing windows and more uniform quality (Baffou and Quidant, 2013). In thermoplasmonic welding with NPs, CW irradiation may cause micro-scale damage to printed circuit films owing to the thermal diffusion in the process (Wang and Ding, 2019). The CW irradiation has inherent problems of high-power consumption and safety concerns, restricting the commercial application.

Pulsed laser irradiation provides high heating efficiency, smaller heat-affected zone, and lower power consumption. It can trigger a localized temperature rise within sub-nanosecond order, further concentrating the temperature rise to the vicinity of NP (Figure 6). The thermodynamics under pulsed illumination is affected by parameters such as pulse duration, frequency, and size of the NP (Baffou and Quidant, 2013). The cooling duration is an important parameter to control the thermal diffusivity and material geometry. At the initial stage of relaxation, the lattice sustains in a hot state, and photons continue to be absorbed to increase the lattice energy (Sundaraman et al., 2014). Within a few ps, the energy distribution is close to thermal equilibrium. For the short laser pulse, thermal diffusion occurs at a timescale of  $10^{-11}\text{ s}$  (Linde et al., 1997). A high heating rate and steep temperature gradient are the characteristics of a laser-matter interaction. When the time interval between pulses is less than the cooling timescale, a very fast pulse repetition rate could increase the baseline temperature (Stockman et al., 2013). Thermoplasmonic welding occurs when the pulse duration is longer than the thermal coupling between the electron gas and the lattice phonons (Chen et al., 2011). Pulse irradiation is more capable of rapidly increasing and decreasing temperature in metal structures, and controlling the thermal distribution of various physical processes in unprecedented space and time. The localization heating have advantages in control, speed,

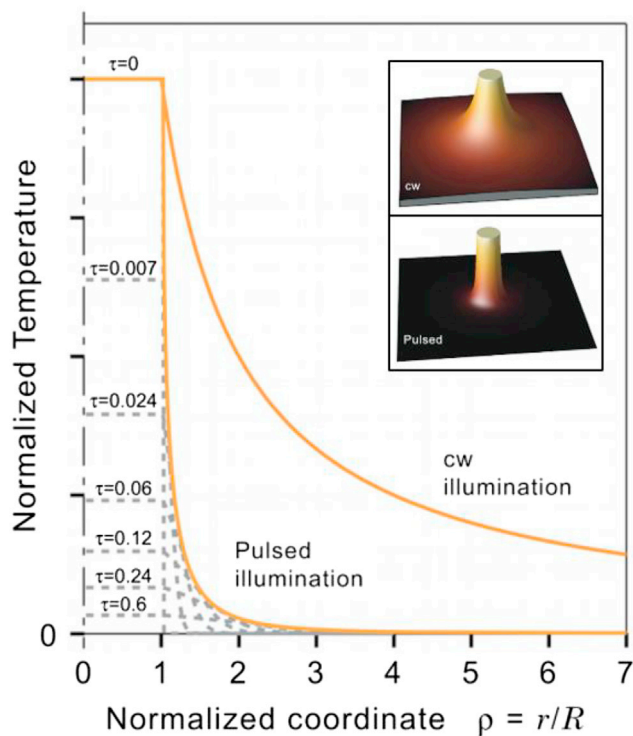


**Figure 6. The temperature profiles upon CW and pulsed illuminations**

Insert: three-dimensional representation of the temperature profile around an NP under CW illumination and femtosecond-pulse illumination. Reprinted and adapted with permission from [Baffou and Quidant \(2013\)](#). Copyright 2012, WILEY-VCH.

and energy efficiency with low costs ([Baffou and Quidant, 2013](#)). Therefore, the pulse laser is the primary choice for welding and metallurgical assembly ([Garnett et al., 2012](#); [Ha et al., 2016](#)).

### Performance characterization

Performance characterization of thermoplasmonic welding is vital to quantify the electrical, mechanical, thermal, and physical properties. Different characterizations are carried out to judge the mechanical and electrical properties. The electrical measurement of nano-welding is realized by measuring the resistance by a nanoprobe manipulator ([Wang et al., 2020](#)). Resistance is a crucial characteristic to evaluate the electrical connection of materials. The four-point probe method accurately measures the sheet resistance because it eliminates the influence of nanomaterials and contact on the overall resistance ([Smits, 1958](#)). It is useful for testing transparent conductive materials, such as thin films or metal NWs ([Papanastasiou et al., 2020](#)). This electrical measurement is valuable for estimating the electrical uniformity by measuring their electrical properties. Two-point probes are also useful in resistance measurement. Two parallel electrodes on opposite sides are made of silver ink or metal layers deposited by evaporation or sputtering. This two-point probe method uses micro tungsten probes to track the resistance measured during voltage or thermal ramp ([Yang et al., 2018](#)). The four-point probe method and the two-point probe method provide similar results for the uniform square layer. Another tool for studying electrical uniformity is single probe electrical mapping and drawing voltage distribution maps ([Zhang et al., 2017](#)).

Mechanical characterization of nano-welding includes theoretical research and experimental measurement. Theoretical studies mainly discuss and analyze the atomic distribution of the joint by molecular dynamics. Compared with high-temperature annealing, welding by light-induced has fewer disordered atoms, phase transitions, dislocations, and smaller residual stresses ([Luan et al., 2020a](#)). However, the research on the evolution of nano-welding behavior on hotspots caused by the plasmon effect on the atomic scale is not mature ([Luan et al., 2020b](#)). In terms of mechanical measurement, there is little research on the direct measurements of joints because it is still limited by the coupling of light-induced processes

and *in-situ* mechanical measurement systems. Researchers used direct fatigue strength and mechanical tensile tests to measure welded nanostructures. The fatigue strength is verified by comparing the resistivity before and after ten million bending cycles. In the cyclic bending test, the resistance of nano-welded conductor changes little after tens of thousands of bending cycles, indicating the welded materials present robust contact (Han et al., 2014). Mechanical tensile experiments are conducted by applying strain and testing extreme bending conditions. For example, it is judged by observing whether the materials crack owing to increased strain. The mechanical strength of welding materials could be verified by hanging. The method can be tested through the suspension of the welding structure by fixing one end of the material and raising the other end to a horizontal plane with an angle of 44° (Ghosh et al., 2019). The results show that the adhesion between the material and the substrate after welding is strong enough to keep together, demonstrating the strong mechanical strength of the welded structure.

## THE EMERGING APPLICATIONS

Thermoplasmonic welding is a promising technology for the interconnection of micro/nano components, which is crucial for fabricating miniature devices and/or systems (An et al., 2014; Angmo et al., 2013). This section summarizes the emerging applications of thermoplasmonic welding in electronic device, optical application, and additive manufacturing.

### Electronic device

Thermoplasmonic welding provides a contactless, damage-free method for precision device fabrication, especially transparent conductive electrodes. Transparent conductive electrodes are often used to collect charges from nearby functional layers or provide carriers to these functional layers so that light can either pass through or absorbed by the devices (Cao et al., 2014; Gordon, 2000). Thermoplasmonic welding provides a direct and repeatable method for making selective electrodes (Yoon and Khang, 2016). Owing to the selectivity of self-limited heating, the NPs welded locally in the overlap area. The metal NWs are considered as material for flexible transparent electrodes with low sheet resistance and high transmittance (Garrett et al., 2012). Specially, Ag NWs and Cu NWs are the potential materials for the next generation of flexible electrodes, including transparent film heaters, displays, and solar cells (Figure 7A) (Celle et al., 2012; Han et al., 2014; Kang et al., 2018).

Ag is one of plasmonic materials with the best conductivity, and it is not easy to generate sparks during welding. In thermoplasmonic welding, Ag NWs are used to fabricate the transparent electrodes as a substitute for expensive ITO (Jang et al., 2018; Seong et al., 2015). The welded AgNWs show stable and strong fluorescence, showing enhanced current density, brightness, and optoelectrical efficiency (Figure 7B) (Liang et al., 2018). The sheet resistance of Ag NWs on a PET substrate achieved 5  $\Omega$ /sq, maintaining an optical transmittance as high as 91%, which is superior to that of any other ITO thin film (<10  $\Omega$ /sq) (Nian et al., 2015). High-performance touch panels and conductive transparent heaters are demonstrated by using this kind of transparent electrode. The metal NP layer serves as a protective layer, preventing transferring of heat to adjacent layers and minimizing the thermal damage to the substrate. It also achieves strong adhesion between metal NW and flexible substrate (Figure 7C). The AgNWs formed by thermoplasmonic welding is subjected to the corresponding peel test, proving that the peel strength before welding reaches 310% (Figure 7D) (Park et al., 2017). Another advantage of AgNWs is that they can use the plasmon effect to improve the performance of the active layer in solar cells and manage light through light harvesting or localization (Cao et al., 2014; Chen et al., 2012a). The partial oxidation and interface layer control the structure and surface function of the plasmon electrode for adjusting the optical and electronic properties. As a low-cost alternative to ITO, the contrast of energy conversion efficiency is slightly reduced (Jose Andres et al., 2015). The power conversion efficiency of hybrid silicon/organic heterojunction photovoltaic devices increased by 35% after welding (Spechler et al., 2015). These results indicate that inexpensive Ag NWs can compete with ITO in photovoltaic technology (Figure 7E).

Copper has been widely used in electronics, with high conductivity and good photoelectric properties. For example, selective welding on Cu NPs to the substrate can manufacture flexible display devices (Kwon et al., 2016). The resistivity of the welded Cu particles is about  $1.67 \times 10^{-4} \Omega \text{ m}$  with an error change below  $\pm 10\%$  in cyclic bending tests (Figure 7F) (Han et al., 2014). The welding structure has good stability that can be connected to the controller as a touch screen device, realizing the direct input on the flexible device. These wide applications benefit from the transparency, conductivity, and flexibility of metal NPs welded by thermoplasmonic heating. In the future, thermoplasmonic welding could be extending applied

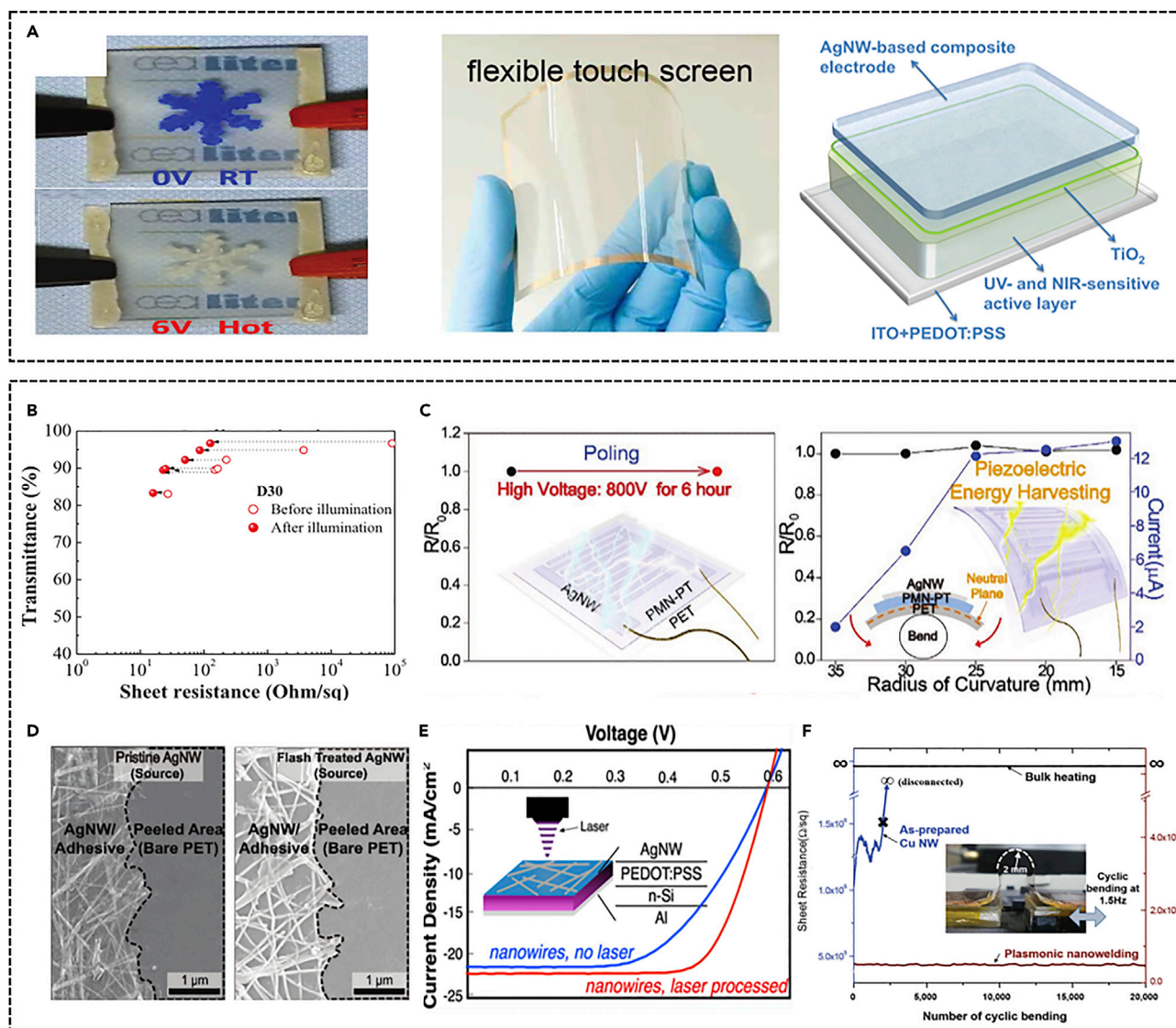


**Figure 7. Thermoplasmonic welding in an electronic device**

(A) Application of welded NWs in transparent film heaters, displays, and solar cells. Reprinted and adapted with permission from Celle et al. (2012), Chen et al. (2012a), and Kang et al. (2018). Copyright 2012, Springer. Copyright 2018, American Chemical Society. Copyright 2017, American Chemical Society. Copyright 2018, WILEY-VCH.

(B) Sheet resistance and transmittance of the AgNWs films before and after illumination. Reprinted and adapted with permission from Liang et al. (2018).

(C) Stable performance and transparent energy harvester of the pressure test.

(D) SEM image of the pristine AgNW/PET film after the peeling test. Reprinted and adapted with permission from Park et al. (2017). Copyright 2016, WILEY-VCH.

(E) J-V characteristic curves for a heterojunction cell. Reprinted and adapted with permission from Spechler et al. (2015). Copyright 2015, American Chemical Society.

(F) The cyclic bending test of the Cu-NW transparent conductor. Reprinted and adapted with permission from Han et al. (2014). Copyright 2014, WILEY-VCH.

to sensors and transistors in bioelectronics, such as piezoresistive strain sensors based on stretchable conductive nanocomposites, wearable sensors that can monitor body movement, touch and pressure changes, etc. (Lee et al., 2016; Yao and Zhu, 2014).

### Optical application

Plasmon-welded structures attract great attention in optical applications. The intrinsic resonance properties and the way of plasmon excitation and propagation can be rationally designed for optical

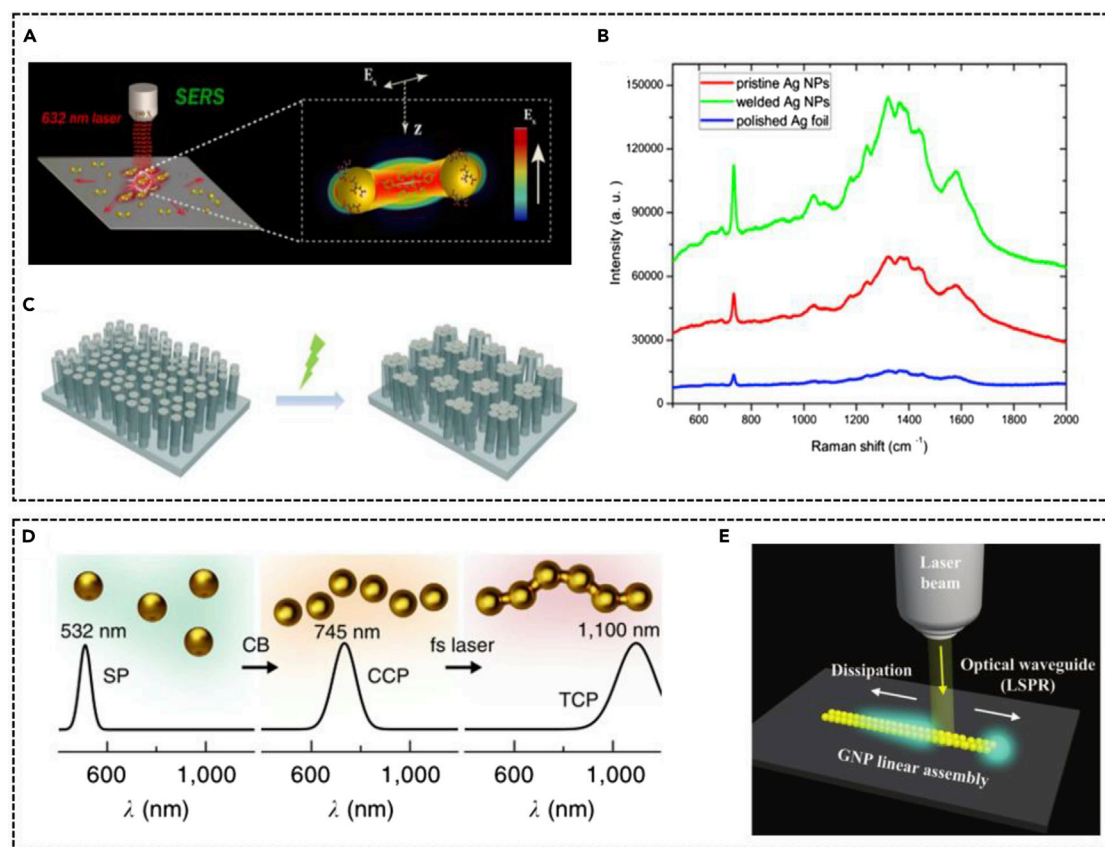


**Figure 8. Thermoplasmonic welding in an optical application**

(A) SERS measurement. Reprinted and adapted with permission from [Dutta and Chattopadhyay \(2017\)](#). Copyright 2017, American Chemical Society.

(B) Raman signal showing the detection of adenine for Ag foil, pristine Ag NPs, and welded Ag NPs. Reprinted and adapted with permission from [Hu et al. \(2012\)](#) Copyright 2012, Laser Institute of America.

(C) The plasmonic gap device. Reprinted and adapted with permission from [Wang et al. \(2016\)](#) Copyright 2016, American Chemical Society.

(D) Chain welding of Au NPs. Reprinted and adapted with permission from [Herrmann et al. \(2014\)](#) Copyright 2014, Macmillan Publishers Limited.

(E) Plasmonic waveguiding along the AuNP linear assembly. Reprinted and adapted with permission from [Su et al. \(2013\)](#) Copyright 2013, WILEY-VCH.

applications, such as surface enhanced Raman spectroscopy (SERS) and plasmon waveguide applications ([Dutta and Chattopadhyay, 2017](#); [Su et al., 2013](#)). SERS is an ideal tool for the detection of trace chemicals in chemical, biomedical and environmental applications ([Figure 8A](#)) ([Le Ru and Etchegoin, 2008](#); [Yamamoto et al., 2014](#)). Plasmonic elements as receiving optical antenna to convert far-field into the near field is an important step to enhance SERS ([Ding et al., 2016](#)). The SERS enhancement factor depends on the size, morphology, and configuration of plasmonic NPs. The enhancement factor value on the order of  $10^7$ – $10^8$  is sufficient for single-molecule detection ([Etchegoin and Le Ru, 2008](#)). Welding metal NPs into an anisotropic structure is one of the ways to improve the detection limit ([Qin et al., 2019](#)). Nie et al. show that anisotropic colloidal metal NPs with high aspect ratio can increase the SERS enhancement factor to  $10^{14}$  ([Nie and Emory, 1997](#)). Multiple NP welding has also been adopted for ultra-sensitive detection, because the plasmon-coupling provides EM field enhancement and amplifies slight changes in a local environment ([Xi et al., 2015](#)). This enhancement leads to vibrational Raman signals that are more intense and stable than single-molecule fluorescence ([Figure 8B](#)) ([Itoh et al., 2013](#); [Slablab et al., 2012](#)). The detection limit of welded Ag NPs enhances five to six times than that of the randomly distributed NPs ([Hu et al., 2012](#)). A smart nanogap device is prepared by studying the dynamic response of Ag nanorod arrays during light irradiation ([Wang et al., 2016](#)). Several nanorods are welded together as a bundle unit owing to the photothermal effect, leading to a sharp increase in the local EM field at bundle tip ([Figure 8C](#)). This bundle tip can be more adjustable to use light as an external stimulus on the nanoscale for SERS detection.

Moreover, the nano-chain structure can transfer surface plasmons polaritons along with the close-packed linear structure (Chen et al., 2019b). The strong near-field coupling and field enhancement effects lead to unidirectional optical transmission along one-dimensional NP chains at sub-wavelength scales. The ordered NP structure act as a waveguide for the directional transfer of photons (Pala et al., 2013). Metal NPs are welded into the one-dimensional chain structure that can obtain a plasmon waveguide, coupling the incident laser beam to realize the directional propagation of light (Figures 8D and 8E) (Herrmann et al., 2014). For applications of the plasmon waveguide, the interparticle oscillation leads to inevitable transport loss (Solis et al., 2012). A wider combination means that there are more NPs at the same distance. The oscillations between isotropic particles waste light energy and limit the propagation distance (Chen et al., 2019b). Reducing the width of NPs' chain is one of the strategies to avoid the transmission loss along the waveguide. For example, when the width of the Ag NPs' chains is shortened to 100 nm, the propagation distance increased slightly by 3.2 mm (Su et al., 2014). These studies show that the thermoplasmonic welding is a fast and cost-effective way of designing and manufacturing optical devices.

### Additive manufacturing

Three-dimensional (3D) printing has developed rapidly in the past decade and is becoming the preferred production mode for many items in daily life. Selective sintering of powder materials by laser heating is one of the effective methods (Yap et al., 2015). However, the range of basic powder materials available is limited, which constitutes the main obstacle to further developing this field. More than 80% of the commercial polymer materials used for laser sintering are polyamide PA12 and its modifications. Owing to its low coupling of laser energy and inefficient manufacturing, it hardly meets the quality requirements (Lau et al., 2014). This technique typically requires high-power CO<sub>2</sub> lasers and remains slow and costly compared with conventional processing methods. That polymer powder mixed with broad light absorption additives acts as a photosensitizer for photothermal welding. At present, most of the materials used are carbon-based nanomaterials, so the printed objects are black or grey, making it impossible to produce colorful parts without many post-processing steps.

The stability and optical response of plasmonic NPs made them ideal candidates for additive manufacturing owing to their long-lasting coloration (Chen et al., 2021). LSPR in metal NPs can adjust absorption peaks from UV to near-infrared by designing the geometry and structure. This phenomenon makes thermoplasmonic welding a potential technology to weld materials at low light power with minimal damage (Figure 9A). As shown in Figure 9B, the color of printed matter depends to some extent on the writing speed of the laser, because this defines the welding degree (Powell et al., 2020). The nanocomposites mixed with the plasmonic materials with polyamide powder could be made into vivid objects, showing colorful effects (Figures 9C and 9D) (Powell et al., 2018). Au NPs have great potential in the aesthetic design of 3D printing, but their high cost is not conducive to large-scale application. Ag NPs are 40 times cheaper than Au, and their molar absorption coefficient at the LSPR peak is four times that of Au. Owing to the LSPR of Ag NPs, the Ag NPs thermoplastic polyurethane composite powder is bright yellow (Hupfeld et al., 2020). Plasmonic NPs thus can be flexible welded under light irradiation to realize multi-color 3D printing. A large number of post-processing steps can be reduced in additive manufacturing, and the application restrictions are alleviated in functional prototyping, and fashion. Therefore, the colorful colors, fast welding speed and low-loss of thermoplasmonic welding provide flexible choices for additive manufacturing.

### CONCLUSIONS AND FUTURE PROSPECTS

Thermoplasmonic welding is an optical method for connecting nano-objects by taking advantage of the extreme field concentration offered by plasmonics. This technology has the advantages of high accuracy and compatibility with flexible devices and provides a new control level for the welding materials. In this review, we overview this novel welding technology based on the distinct features of thermoplasmonics. The physical mechanism is discussed with focus on the photothermal effect, self-limited heating, as well as the melting and solidification process. Key aspects of the welding are considered from the optical and thermal aspects, including the material scrutinization, geometric and spatial configuration, heat scheme, and performance characterization. Finally, the potential applications of this technology are highlighted in electrical devices, optical applications and manufacturing field. Overall, the thermoplasmonic welding supports mechanical connections between different nanocomponents and diverse functional devices. This technology has been widely used in the additive manufacturing and connection of nanostructures with diverse materials, the assembly of integrated circuits and electronic devices etc. Table 1 summarizes the state-of-the-art methods used in nano-welding, and briefly lists its working mechanism, materials,

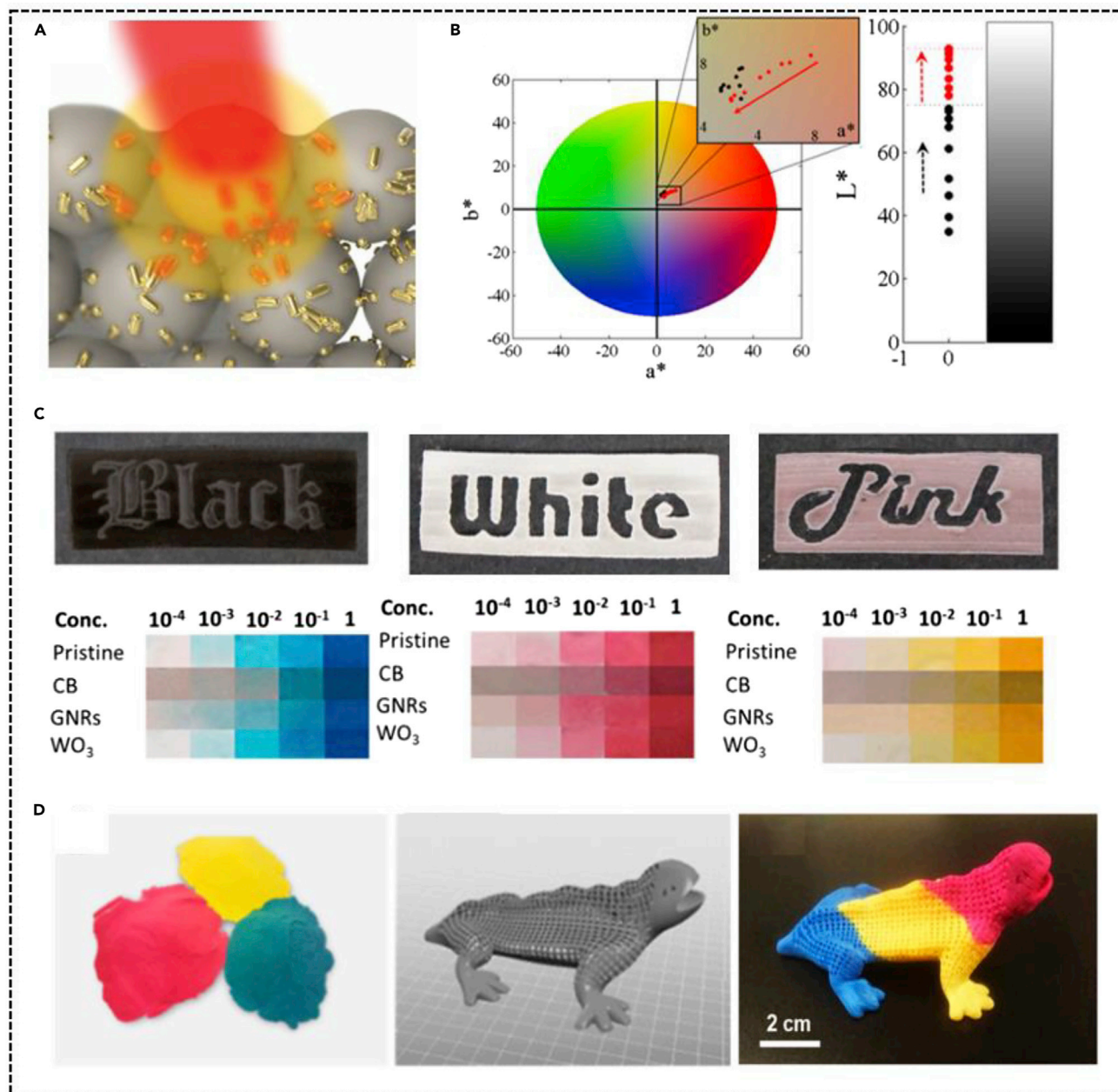


**Figure 9. Thermoplasmonic welding in additive manufacturing**

(A) The heating effect of Au NPs.

(B) The hue ( $a^*$  and  $b^*$ ) and brightness ( $L^*$ ) of black and Au nanorods (red) welded at different scan speeds.

(C) Welded samples produced with different materials. Reprinted and adapted with permission from Powell et al. (2020) Copyright 2020, American Chemical Society.

(D) Colored powders used to make the colorful objects. Reprinted and adapted with permission from Powell et al. (2018) Copyright 2018, American Chemical Society.

and challenges. Thermoplasmonic welding has the advantages of simple operation, high welding efficiency and accuracy with minimum thermal damage. However, as a fusion welding method, there are some restrictions of the technique. Plasmonic heating must be present for the welding materials. Owing to the inverse effect of hotspots, the welding quality depends on the irradiation duration, light intensity, and interface geometry.

**Table 1. Nanowelding methods, working principle, materials, and challenges**

Methods		Working principle	Materials	Challenges	Ref
Solid-state welding	Pressure joining	External force is applied through ultrasonic vibration, normal compression, nanoindentation, etc.	Metal/Semiconductor/ Ceramic 2D materials, etc.	Difficult to control deformation degree, low accuracy	(Krzanowski, 1989; Lin et al., 2015; Peng et al., 2017)
	Cold welding	The diffusion barrier of a single metal atom on a clean metal surface is very low, and even a small thermal activation is enough to trigger atomic diffusion. When two clean interfaces are close, mutual diffusion will occur automatically.	Ultrathin metallic materials	Complex operation, less applicable materials	(Dai et al., 2016; Liu et al., 2017; Wagle and Baker, 2015)
Brazing		Molten filler is introduced between components to form joints. The solid material dissolves and diffuses into the molten liquid in the joint, accompanied by the formation of a reaction zone.	Metal/Semiconductor/ Ceramic 2D materials, etc.	Complex operation, low welding efficiency	(Gao and Gu, 2010; Gu et al., 2005; Peng et al., 2009)

(Continued on next page)

**Table 1. Continued**

Methods		Working principle	Materials	Challenges	Ref
Fusion welding	Joule heating	Welding is carried out by accurately controlling the contact geometry and current between materials. When contact is formed, a hotspot is generated at the contact point owing to the high local current density.	Metal materials	Complex operation, thermal damage. less applicable materials	(Chellattoan et al., 2019; Song et al., 2014; Tohmyoh et al., 2007)
	Electron beam welding	It refers to the impact of high-speed beam on the material surface under vacuum, and most of its energy is converted into heat energy in a fraction of a microsecond.	Metal/Semiconductor/ Ceramic 2D materials, etc.	High cost, complex equipment	(Koleva, 2005; Terrones et al., 2002; Zhang et al., 2018)
	Ultrafast laser welding	Using a pulse width much smaller than the electron lattice thermal coupling time, electrons do not have enough time to transfer energy to the lattice. The excited electrons are thrown out, weakening the chemical bonds of lattice atoms and causing the atoms on the surface of the material to melt.	Metal/Semiconductor/ Ceramic 2D materials, etc.	long irradiation time (>1 min), high laser fluence	(Gonzalez-Rubio et al., 2017; Huang et al., 2012; Itoh et al., 2013)
	Thermoplasmonic welding	Light-matter interaction via nano gaps of materials results in enhancement of the electromagnetic field, effectively concentrating heat at the desired point where the materials to be welded together.	Metal/Semiconductor 2D materials, etc.	Plasmonic material must be present, affected by hotspot sizes	(Garnett et al., 2012; Jang et al., 2018; Park et al., 2017)

In the future, thermoplasmonic welding can be further developed from several aspects such as heterogeneous welding, new structured materials, and other potential applications. So far, thermoplasmonic welding mainly focus on the homogeneous junction, whereas the heterogeneous welding research is less. Therefore, the relationships between plasmonic materials and semiconductors, ceramics, and other materials need further investigation. These hybrid structures composed of heterogeneous materials create hotspots with diverse local field enhancements, which may be conducive or detrimental to concentrate light and heat for self-limiting welding (Ding et al., 2016, 2017). Multi-interface plasmon-coupling in metal-semiconductor core-shell structure has been prepared by thermoplasmonic welding with semiconductors as spacer material (Liu and Xue, 2021). Compared with NP contact, this strategy provides a large hotspot volume covering the whole semiconductor spacer by the strong plasmon-coupling between the metal NP core and the decorative metal NP on the semiconductor shell (Alkurdi et al., 2020; Hardiansyah et al., 2015). Future work using thermoplasmonic welding may allow other new applications in biology, aerospace, and other fields such as self-powered window displays or touch-sensitive screen at a very low cost. With the deepening of our understanding on thermoplasmonic welding, we believe that this technology would inspire new translation into the manufacturing field toward a better future.

## ACKNOWLEDGMENTS

This research was supported by the Natural Science Foundation of China (52076077).

## AUTHOR CONTRIBUTIONS

Conceptualization: G.L. and L.W.; visualization: L.W. and Y.F.; writing – original draft: L.W. and Y.F.; writing – review and editing: L.W., Y.F., and Z.L.; copyright: L.W., Y.F., and Z.L.; funding acquisition: G.L.; supervision: G.L.

## DECLARATION OF INTERESTS

The authors declare no competing interests.

## REFERENCES

- Hu, A., Peng, P., Alarifi, H., Zhang, X.Y., Guo, J.Y., Zhou, Y., and Duley, W.W. (2012). Femtosecond laser welded nanostructures and plasmonic devices. *J. Laser Appl.* 24, 042001. <https://doi.org/10.2351/1.3695174>.
- Alkurdi, A., Lombard, J., Detcheverry, F., and Merabia, S. (2020). Enhanced heat transfer with metal-dielectric core-shell nanoparticles. *Phys. Rev. Appl.* 13, 034036. <https://doi.org/10.1103/PhysRevApplied.13.034036>.
- An, K., Hong, S., Han, S., Lee, H., Yeo, J., and Ko, S.H. (2014). Selective sintering of metal nanoparticle ink for maskless fabrication of an electrode micropattern using a spatially modulated laser beam by a digital micromirror device. *ACS Appl. Mater. Interfaces* 6, 2786–2790. <https://doi.org/10.1021/am405323c>.
- Angmo, D., Larsen-Olsen, T.T., Jørgensen, M., Søndergaard, R.R., and Krebs, F.C. (2013). Roll-to-roll Inkjet printing and photonic sintering of electrodes for ITO free polymer solar cell modules and facile product integration. *Adv. Energy Mater.* 3, 172–175. <https://doi.org/10.1002/aenm.201200520>.
- Baffou, G., Quidant, R., and Girard, C. (2010). Thermoplasmonics modeling: a Green's function approach. *Phys. Rev. B* 82, 165424. <https://doi.org/10.1103/PhysRevB.82.165424>.
- Baffou, G., and Quidant, R. (2013). Thermoplasmonics: using metallic nanostructures as nano-sources of heat. *Laser Photon. Rev.* 7, 171–187. <https://doi.org/10.1002/lpor.201200003>.
- Baffou, G., and Quidant, R. (2014). Nanoplasmonics for chemistry. *Chem. Soc. Rev.* 43, 3898–3907. <https://doi.org/10.1039/c3cs60364d>.
- Baljon, A.R.C., and Robbins, M.O. (1996). Energy dissipation during rupture of adhesive bonds. *Science* 271, 482–484. <https://doi.org/10.1126/science.271.5248.482>.
- Bauerle, D. (2011). Nucleation and cluster formation. In *Laser Processing and Chemistry* (Springer), pp. 63–83.
- Brongersma, M.L., Halas, N.J., and Nordlander, P. (2015). Plasmon-induced hot carrier science and technology. *Nat. Nanotechnol.* 10, 25–34. <https://doi.org/10.1038/nnano.2014.311>.
- Cao, W., Li, J., Chen, H., and Xue, J. (2014). Transparent electrodes for organic optoelectronic devices: a review. *J. Photon. Energy* 4, 040990. <https://doi.org/10.1117/1.Jpe.4.040990>.
- Celle, C., Mayousse, C., Moreau, E., Basti, H., Carella, A., and Simonato, J.-P. (2012). Highly flexible transparent film heaters based on random networks of silver nanowires. *Nano Res.* 5, 427–433. <https://doi.org/10.1007/s12274-012-0225-2>.
- Chan, G.H., Zhao, J., Hicks, E.M., Schatz, G.C., and Van Duyne, R.P. (2007). Plasmonic properties of copper nanoparticles fabricated by nanosphere lithography. *Nano Lett.* 7, 1947–1952. <https://doi.org/10.1021/nl070648a>.
- Changsoo Kim, P.E.B., Burrows, P.E., Forres, S.R., and Forrest, S.R. (2000). Micropatterning of organic electronic devices by cold-welding. *Science* 288, 831–833. <https://doi.org/10.1126/science.288.5467.831>.
- Chellattoan, R., Lube, V., and Lubineau, G. (2019). Toward programmable materials for wearable electronics: electrical welding turns sensors into conductors. *Adv. Electron. Mater.* 5, 1800273. <https://doi.org/10.1002/aeml.201800273>.
- Chen, C., Kuang, Y., and Hu, L. (2019a). Challenges and opportunities for solar evaporation. *Joule* 3, 683–718. <https://doi.org/10.1016/j.joule.2018.12.023>.
- Chen, C.C., Dou, L., Zhu, R., Chung, C.H., Song, T.B., Zheng, Y.B., Hawks, S., Li, G., Weiss, P.S., and Yang, Y. (2012a). Visibly transparent polymer solar cells produced by solution processing. *ACS Nano* 6, 7185–7190. <https://doi.org/10.1021/nm3029327>.
- Chen, H., Shao, L., Ming, T., Sun, Z., Zhao, C., Yang, B., and Wang, J. (2010). Understanding the photothermal conversion efficiency of gold nanocrystals. *Small* 6, 2272–2280. <https://doi.org/10.1002/sml.201001109>.
- Chen, H., Shao, L., Li, Q., and Wang, J. (2013). Gold nanorods and their plasmonic properties. *Chem. Soc. Rev.* 42, 2679–2724. <https://doi.org/10.1039/c2cs35367a>.
- Chen, J., Chen, W.K., Tang, J., and Rentzepis, P.M. (2011). Time-resolved structural dynamics of thin metal films heated with femtosecond optical

- pulses. *Proc. Natl. Acad. Sci. U S A* 108, 18887–18892. <https://doi.org/10.1073/pnas.1115237108>.
- Chen, J., Ye, Z., Yang, F., and Yin, Y. (2021). Plasmonic nanostructures for photothermal conversion. *Small Science* 1, 2000055. <https://doi.org/10.1002/smcs.202000055>.
- Chen, L., Su, B., and Jiang, L. (2019b). Recent advances in one-dimensional assembly of nanoparticles. *Chem. Soc. Rev.* 48, 8–21. <https://doi.org/10.1039/c8cs00703a>.
- Chen, X., Chen, Y., Yan, M., and Qiu, M. (2012b). Nanosecond photothermal effects in plasmonic nanostructures. *ACS Nano* 6, 2550–2557. <https://doi.org/10.1021/nl20500032>.
- Cunha, J., Guo, T.L., Della Valle, G., Koya, A.N., Proietti Zaccaria, R., and Alabastri, A. (2020). Controlling light, heat, and vibrations in plasmonics and phononics. *Adv. Opt. Mater.* 8, 2001225. <https://doi.org/10.1002/adom.202001225>.
- Dai, G., Wang, B., Xu, S., Lu, Y., and Shen, Y. (2016). Side-to-side cold welding for controllable nanogap formation from "dumbbell" ultrathin gold nanorods. *ACS Appl. Mater. Interfaces* 8, 13506–13511. <https://doi.org/10.1021/acsami.6b01070>.
- DebRoy, T., Wei, H.L., Zuback, J.S., Mukherjee, T., Elmer, J.W., Milewski, J.O., Beese, A.M., Wilson-Heid, A., De, A., and Zhang, W. (2018). Additive manufacturing of metallic components - process, structure and properties. *Prog. Mater. Sci.* 92, 112–224. <https://doi.org/10.1016/j.pmatsci.2017.10.001>.
- Deng, Y., Bai, Y., Yu, Y., Deng, S., Tian, Y., Zhang, G., Zheng, C., Wu, J., and Hu, A. (2019). Laser nanojoining of copper nanowires. *J. Laser Appl.* 31, 022414. <https://doi.org/10.2351/1.5096137>.
- Ding, S., Yi, J., Li, J.F., Ren, B., Wu, D.Y., Panneerselvam, R., and Tian, Z.Q. (2016). Nanostructure-based plasmon-enhanced Raman spectroscopy for surface analysis of materials. *Nat. Rev. Mater.* 1, 16021. <https://doi.org/10.1038/natrevmats.2016.21>.
- Ding, S.Y., You, E.M., Tian, Z.Q., and Moskovits, M. (2017). Electromagnetic theories of surface-enhanced Raman spectroscopy. *Chem. Soc. Rev.* 46, 4042–4076. <https://doi.org/10.1039/c7cs00238f>.
- Dutta, A., and Chattopadhyay, A. (2017). Surface and tip-enhanced Raman spectroscopy at the plasmonic hot spot of a coordination complex-conjugated gold nanoparticle dimer. *J. Phys. Chem. C* 121, 18854–18861. <https://doi.org/10.1021/acs.jpcc.7b07301>.
- Emanuele Lio, G., De Luca, A., Umeton, C.P., and Caputo, R. (2020). Opto-mechanically induced thermoplasmonic response of unclonable flexible tags with hotspot fingerprint. *J. Appl. Phys.* 128, 093107. <https://doi.org/10.1063/5.0018992>.
- Eom, H.J. (2004). *Electromagnetic Wave Theory for Boundary-Value Problems* (Springer).
- Etchegoin, P.G., and Le Ru, E.C. (2008). A perspective on single molecule SERS: current status and future challenges. *Phys. Chem. Chem. Phys.* 10, 6079–6089. <https://doi.org/10.1039/b809196j>.
- Eustis, S., and el-Sayed, M.A. (2006). Why gold nanoparticles are more precious than pretty gold: noble metal surface plasmon resonance and its enhancement of the radiative and nonradiative properties of nanocrystals of different shapes. *Chem. Soc. Rev.* 35, 209–217. <https://doi.org/10.1039/b514191e>.
- Gao, F., and Gu, Z. (2010). Nano-soldering of magnetically aligned three-dimensional nanowire networks. *Nanotechnology* 21, 115604. <https://doi.org/10.1088/0957-4484/21/11/115604>.
- Garnett, E.C., Cai, W., Cha, J.J., Mahmood, F., Connor, S.T., Greyson Christoforo, M., Cui, Y., McGehee, M.D., and Brongersma, M.L. (2012). Self-limited plasmonic welding of silver nanowire junctions. *Nat. Mater.* 11, 241–249. <https://doi.org/10.1038/nmat3238>.
- Ghosh, P., Lu, J., Luo, H., Wang, W., Xu, Z., Qiu, M., and Li, Q. (2019). Constructing metal arch nanobridges utilizing a photothermal-induced nanobonding technique. *Adv. Electron. Mater.* 5, 1800807. <https://doi.org/10.1002/aelm.201800807>.
- Giannini, V., Fernandez-Dominguez, A.I., Sonnefraud, Y., Roschuk, T., Fernandez-Garcia, R., and Maier, S.A. (2010). Controlling light localization and light-matter interactions with nanoplasmonics. *Small* 6, 2498–2507. <https://doi.org/10.1002/sml.201001044>.
- Gonzalez-Rubio, G., Diaz-Nunez, P., Rivera, A., Prada, A., Tardajos, G., Gonzalez-Izquierdo, J., Banares, L., Llombart, P., Macdowell, L.G., Alcolea Palafox, M., et al. (2017). Femtosecond laser reshaping yields gold nanorods with ultranarrow surface plasmon resonances. *Science* 358, 640–644. <https://doi.org/10.1126/science.aan8478>.
- Gordon, R.G. (2000). Criteria for choosing transparent conductors. *MRS Bull.* 25, 52–57. <https://doi.org/10.1557/mrs2000.151>.
- Govorov, A.O., and Richardson, H.H. (2007). Generating heat with metal nanoparticles. *Nano Today* 2, 30–38. [https://doi.org/10.1016/s1748-0132\(07\)70017-8](https://doi.org/10.1016/s1748-0132(07)70017-8).
- Gu, Z., Ye, H., and Gracias, D.H. (2005). The bonding of nanowire assemblies using adhesive and solder. *JOM* 57, 60–64. <https://doi.org/10.1007/s11837-005-0185-z>.
- Ha, J., Lee, B.J., Hwang, D.J., and Kim, D. (2016). Femtosecond laser nanowelding of silver nanowires for transparent conductive electrodes. *RSC Adv.* 6, 86232–86239. <https://doi.org/10.1039/c6ra19608j>.
- Ha, M., Kim, J.H., You, M., Li, Q., Fan, C., and Nam, J.M. (2019). Multicomponent plasmonic nanoparticles: from heterostructured nanoparticles to colloidal composite nanostructures. *Chem. Rev.* 119, 12208–12278. <https://doi.org/10.1021/acs.chemrev.9b00234>.
- Halas, N.J., Lal, S., Chang, W.S., Link, S., and Nordlander, P. (2011). Plasmons in strongly coupled metallic nanostructures. *Chem. Rev.* 111, 3913–3961. <https://doi.org/10.1021/cr200061k>.
- Han, S., Hong, S., Ham, J., Yeo, J., Lee, J., Kang, B., Lee, P., Kwon, J., Lee, S.S., Yang, M.Y., and Ko, S.H. (2014). Fast plasmonic laser nanowelding for a Cu-nanowire percolation network for flexible transparent conductors and stretchable electronics. *Adv. Mater.* 26, 5808–5814. <https://doi.org/10.1002/adma.201400474>.
- Hardiansyah, A., Chen, A.Y., Liao, H.L., Yang, M.C., Liu, T.Y., Chan, T.Y., Tsou, H.M., Kuo, C.Y., Wang, J.K., and Wang, Y.L. (2015). Core-shell of FePt@SiO<sub>2</sub>-Au magnetic nanoparticles for rapid SERS detection. *Nanoscale Res. Lett.* 10, 412. <https://doi.org/10.1186/s11671-015-1111-0>.
- Hartland, G.V. (2011). Optical studies of dynamics in noble metal nanostructures. *Chem. Rev.* 111, 3858–3887. <https://doi.org/10.1021/cr1002547>.
- Herrmann, L.O., Valev, V.K., Tserkezis, C., Barnard, J.S., Kasper, S., Scherman, O.A., Aizpurua, J., and Baumberg, J.J. (2014). Threading plasmonic nanoparticle strings with light. *Nat. Commun.* 5, 4568. <https://doi.org/10.1038/ncomms5568>.
- Huang, H., Liu, L., Peng, P., Hu, A., Duley, W.W., and Zhou, Y. (2012). Controlled joining of Ag nanoparticles with femtosecond laser radiation. *J. Appl. Phys.* 112, 123519. <https://doi.org/10.1063/1.4770476>.
- Hupfeld, T., Wegner, A., Blanke, M., Doñate-Buendia, C., Sharov, V., Nieskens, S., Piechotta, M., Giese, M., Barcikowski, S., and Gökce, B. (2020). Plasmonic seasoning giving color to desktop laser 3D printed polymers by highly dispersed nanoparticles. *Adv. Opt. Mater.* 8, 2000473. <https://doi.org/10.1002/adom.202000473>.
- Itoh, T., Yamamoto, Y.S., Tamaru, H., Biju, V., Murase, N., and Ozaki, Y. (2013). Excitation laser energy dependence of surface-enhanced fluorescence showing plasmon-induced ultrafast electronic dynamics in dye molecules. *Phys. Rev. B* 87, 235408. <https://doi.org/10.1103/PhysRevB.87.235408>.
- Jang, Y.R., Chung, W.H., Hwang, Y.T., Hwang, H.J., Kim, S.H., and Kim, H.S. (2018). Selective wavelength plasmonic flash light welding of silver nanowires for transparent electrodes with high conductivity. *ACS Appl. Mater. Interfaces* 10, 24099–24107. <https://doi.org/10.1021/acsami.8b03917>.
- Jauffred, L., Samadi, A., Klingberg, H., Bendix, P.M., and Oddershede, L.B. (2019). Plasmonic heating of nanostructures. *Chem. Rev.* 119, 8087–8130. <https://doi.org/10.1021/acs.chemrev.8b00738>.
- Jiang, K., Smith, D.A., and Pinchuk, A. (2013). Size-dependent photothermal conversion efficiencies of plasmonically heated gold nanoparticles. *J. Phys. Chem. C* 117, 27073–27080. <https://doi.org/10.1021/jp409067h>.
- Jose Andres, L., Fe Menendez, M., Gomez, D., Luisa Martinez, A., Bristow, N., Paul Kettle, J., Menendez, A., and Ruiz, B. (2015). Rapid synthesis of ultra-long silver nanowires for tailor-made transparent conductive electrodes: proof of concept in organic solar cells. *Nanotechnology* 26, 265201. <https://doi.org/10.1088/0957-4484/26/26/265201>.

- Kang, H., Song, S.J., Sul, Y.E., An, B.S., Yin, Z., Choi, Y., Pu, L., Yang, C.W., Kim, Y.S., Cho, S.M., et al. (2018). Epitaxial-growth-induced junction welding of silver nanowire network electrodes. *ACS Nano* 12, 4894–4902. <https://doi.org/10.1021/acsnano.8b01900>.
- Karim, S., Toimil-Molares, M.E., Balogh, A.G., Ensinger, W., Cornelius, T.W., Khan, E.U., and Neumann, R. (2006). Morphological evolution of Au nanowires controlled by Rayleigh instability. *Nanotechnology* 17, 5954–5959. <https://doi.org/10.1088/0957-4484/17/24/009>.
- Kim, A., Won, Y., Woo, K., Kim, C.-H., and Moon, J. (2013). Highly transparent low resistance ZnO/Ag nanowire/ZnO composite electrode for thin film solar cells. *ACS Nano* 7, 1081–1091. <https://doi.org/10.1021/nn305491x>.
- Klinkova, A., Choueiri, R.M., and Kumacheva, E. (2014). Self-assembled plasmonic nanostructures. *Chem. Soc. Rev.* 43, 3976–3991. <https://doi.org/10.1039/c3cs60341e>.
- Knight, M.W., Liu, L., Wang, Y., Brown, L., Mukherjee, S., King, N.S., Everitt, H.O., Nordlander, P., and Halas, N.J. (2012). Aluminum plasmonic nanoantennas. *Nano Lett.* 12, 6000–6004. <https://doi.org/10.1021/nl303517v>.
- Ko, S.H., Pan, H., Grigoropoulos, C.P., Luscombe, C.K., Fréchet, J.M.J., and Poulidakos, D. (2007). Air stable high resolution organic transistors by selective laser sintering of ink-jet printed metal nanoparticles. *Appl. Phys. Lett.* 90, 141103. <https://doi.org/10.1063/1.2719162>.
- Koleva, E. (2005). Electron beam weld parameters and thermal efficiency improvement. *Vacuum* 77, 413–421. <https://doi.org/10.1016/j.vacuum.2004.09.002>.
- Kou, S. (2003). *Welding Metallurgy, Second* (John Wiley & Sons, Inc.).
- Kreibig, U., and Vollmer, M. (1995). Theoretical considerations. In *Optical properties of metal clusters*, U. Kreibig and M. Vollmer, eds. (Springer Berlin Heidelberg), pp. 13–201.
- Krzanowski, J.E. (1989). A transmission electron microscopy study of ultrasonic wire bonding. *IEEE Trans. Compon. Packag. Manuf. Technol.* 13, 176–181. <https://doi.org/10.1109/33.52867>.
- Kwon, J., Cho, H., Eom, H., Lee, H., Suh, Y.D., Moon, H., Shin, J., Hong, S., and Ko, S.H. (2016). Low-temperature oxidation-free selective laser sintering of Cu nanoparticle paste on a polymer substrate for the flexible touch panel applications. *ACS Appl. Mater. Interfaces* 8, 11575–11582. <https://doi.org/10.1021/acsnano.5b12714>.
- Lalisse, A., Tessier, G., Plain, J., and Baffou, G. (2015). Quantifying the efficiency of plasmonic materials for near-field enhancement and photothermal conversion. *J. Phys. Chem. C* 119, 25518–25528. <https://doi.org/10.1021/acs.jpcc.5b09294>.
- Lau, M., Niemann, R.G., Bartsch, M., O'Neill, W., and Barcikowski, S. (2014). Near-field-enhanced, off-resonant laser sintering of semiconductor particles for additive manufacturing of dispersed Au–ZnO-micro/nano hybrid structures. *Appl. Phys. A* 114, 1023–1030. <https://doi.org/10.1007/s00339-014-8270-1>.
- Le Ru, E., and Etchegoin, P. (2008). *Principles of Surface-Enhanced Raman Spectroscopy: And Related Plasmonic Effects* (Elsevier).
- Le Ru, E.C., and Etchegoin, P.G. (2012). Single-molecule surface-enhanced Raman spectroscopy. *Annu. Rev. Phys. Chem.* 63, 65–87. <https://doi.org/10.1146/annurev-physchem-032511-143757>.
- Lecarme, O., Sun, Q., Ueno, K., and Misawa, H. (2014). Robust and versatile light absorption at near-infrared wavelengths by plasmonic aluminum nanorods. *ACS Photonics* 1, 538–546. <https://doi.org/10.1021/ph500096q>.
- Lee, C., Oh, Y., Yoon, I.S., Kim, S.H., Ju, B.K., and Hong, J.M. (2018). Flash-induced nanowelding of silver nanowire networks for transparent stretchable electrochromic devices. *Sci. Rep.* 8, 2763. <https://doi.org/10.1038/s41598-018-20368-3>.
- Lee, J.H., Huynh-Nguyen, B.-C., Ko, E., Kim, J.H., and Seong, G.H. (2016). Fabrication of flexible, transparent silver nanowire electrodes for amperometric detection of hydrogen peroxide. *Sens. Actuator. B Chem.* 224, 789–797. <https://doi.org/10.1016/j.snb.2015.11.006>.
- Liang, X., Lu, J., Zhao, T., Yu, X., Jiang, Q., Hu, Y., Zhu, P., Sun, R., and Wong, C.P. (2018). Facile and efficient welding of silver nanowires based on UVA-induced nanoscale photothermal process for roll-to-roll manufacturing of high-performance transparent conducting films. *Adv. Mater. Interfac.* 6, 1801635. <https://doi.org/10.1002/admi.201801635>.
- Lin, Z., Gui, X., Gan, Q., Chen, W., Cheng, X., Liu, M., Zhu, Y., Yang, Y., Cao, A., and Tang, Z. (2015). In-situ welding carbon nanotubes into a porous solid with super-high compressive strength and fatigue resistance. *Sci. Rep.* 5, 11336. <https://doi.org/10.1038/srep11336>.
- von der Linde, D., Sokolowski-Tinten, K., and Bialkowski, J. (1997). Laser-solid interaction in the femtosecond time regime. *Appl. Surf. Sci.* 109–110, 1–10. [https://doi.org/10.1016/S0169-4332\(96\)00611-3](https://doi.org/10.1016/S0169-4332(96)00611-3).
- Liu, D., and Xue, C. (2021). Plasmonic coupling architectures for enhanced photocatalysis. *Adv. Mater.* 33, e2005738. <https://doi.org/10.1002/adma.202005738>.
- Liu, G., Chen, T., Xu, J., Li, G., and Wang, K. (2020). Solar evaporation for simultaneous steam and power generation. *J. Mater. Chem. A* 8, 513–531. <https://doi.org/10.1039/c9ta12211g>.
- Liu, H.B., Ascencio, J.A., Perez-Alvarez, M., and Yacaman, M.J. (2001). Melting behavior of nanometer sized gold isomers. *Surf. Sci.* 491, 88–98. [https://doi.org/10.1016/S0039-6028\(01\)01351-6](https://doi.org/10.1016/S0039-6028(01)01351-6).
- Liu, Y., Zhang, J., Gao, H., Wang, Y., Liu, Q., Huang, S., Guo, C.F., and Ren, Z. (2017). Capillary-force-induced cold welding in silver-nanowire-based flexible transparent electrodes. *Nano Lett.* 17, 1090–1096. <https://doi.org/10.1021/acs.nanolett.6b04613>.
- Lu, Y., Huang, J.Y., Wang, C., Sun, S., and Lou, J. (2010). Cold welding of ultrathin gold nanowires. *Nat. Nanotechnol.* 5, 218–224. <https://doi.org/10.1038/nnano.2010.4>.
- Luan, S., Yu, S., Gui, C., and Zhou, S. (2020a). Atomic-scale structural evolution and welding deformations of laser welded joints in Ag nanowire connectors on homogeneous substrates. *Jpn. J. Appl. Phys.* 59, 115002. <https://doi.org/10.35848/1347-4065/abc02b>.
- Luan, S., Zhao, Q., Gui, C., and Zhou, S. (2020b). Welding deformations of welded joints between 1D Ag nanowire connectors and 3D substrates: a molecular dynamics study. *Jpn. J. Appl. Phys.* 60, 015004. <https://doi.org/10.35848/1347-4065/abd114>.
- Ma, H., Tian, P., Pello, J., Bendix, P.M., and Oddershede, L.B. (2014). Heat generation by irradiated complex composite nanostructures. *Nano Lett.* 14, 612–619. <https://doi.org/10.1021/nl403798j>.
- Mafune, F., Kohno, J.y., Takeda, Y., and Kondow, T. (2003). Nanoscale soldering of metal nanoparticles for construction of higher-order structures. *J. Am. Chem. Soc.* 125, 1686–1687. <https://doi.org/10.1021/ja021250d>.
- McMahon, J.M., Schatz, G.C., and Gray, S.K. (2013). Plasmonics in the ultraviolet with the poor metals Al, Ga, In, Sn, Ti, Pb, and Bi. *Phys. Chem. Chem. Phys.* 15, 5415–5423. <https://doi.org/10.1039/c3cp43856b>.
- McMahon, M.D., Lopez, R., Meyer, H.M., Feldman, L.C., and Haglund, R.F. (2005). Rapid tarnishing of silver nanoparticles in ambient laboratory air. *Appl. Phys. B* 80, 915–921. <https://doi.org/10.1007/s00340-005-1793-6>.
- Murray, W.A., and Barnes, W.L. (2007). Plasmonic materials. *Adv. Mater.* 19, 3771–3782. <https://doi.org/10.1002/adma.200700678>.
- Nian, Q., Saei, M., Xu, Y., Sabyasachi, G., Deng, B., Chen, Y.P., and Cheng, G.J. (2015). Crystalline nanojoining silver nanowire percolated networks on flexible substrate. *ACS Nano* 9, 10018–10031. <https://doi.org/10.1021/acsnano.5b03601>.
- Nie, S., and Emory, S.R. (1997). Probing single molecules and single nanoparticles by surface-enhanced Raman scattering. *Science* 275, 1102–1106. <https://doi.org/10.1126/science.275.5303.1102>.
- Oliveira, J.P., Santos, T.G., and Miranda, R.M. (2020). Revisiting fundamental welding concepts to improve additive manufacturing: from theory to practice. *Prog. Mater. Sci.* 107, 100590. <https://doi.org/10.1016/j.pmatsci.2019.100590>.
- Pala, R.A., Liu, J.S.Q., Barnard, E.S., Askarov, D., Garnett, E.C., Fan, S., and Brongersma, M.L. (2013). Optimization of non-periodic plasmonic light-trapping layers for thin-film solar cells. *Nat. Commun.* 4, 2095. <https://doi.org/10.1038/ncomms3095>.
- Pan, H., Ko, S.H., and Grigoropoulos, C.P. (2007). The coalescence of supported gold nanoparticles induced by nanosecond laser irradiation. *Appl. Phys. A* 90, 247–253. <https://doi.org/10.1007/s00339-007-4320-2>.
- Papanastasiou, D.T., Schultheiss, A., Muñoz-Rojas, D., Celle, C., Carella, A., Simonato, J.P., and Bellet, D. (2020). Transparent heaters: a review. *Adv. Funct. Mater.* 30, 1910225. <https://doi.org/10.1002/adfm.201910225>.

- Park, J.H., Ambwani, P., Manno, M., Lindquist, N.C., Nagpal, P., Oh, S.H., Leighton, C., and Norris, D.J. (2012). Single-crystalline silver films for plasmonics. *Adv. Mater.* 24, 3988–3992. <https://doi.org/10.1002/adma.201200812>.
- Park, J.H., Jeong, S., Lee, E.J., Lee, S.S., Seok, J.Y., Yang, M., Choi, Y., and Kang, B. (2016). Transversally extended laser plasmonic welding for oxidation-free copper fabrication toward high-fidelity optoelectronics. *Chem. Mater.* 28, 4151–4159. <https://doi.org/10.1021/acs.chemmater.6b00013>.
- Park, J.H., Hwang, G.T., Kim, S., Seo, J., Park, H.J., Yu, K., Kim, T.S., and Lee, K.J. (2017). Flash-induced self-limited plasmonic welding of silver nanowire network for transparent flexible energy harvester. *Adv. Mater.* 29, 1603473–1603479. <https://doi.org/10.1002/adma.201603473>.
- Patolsky, F., Weizmann, Y., and Willner, I. (2004). Actin-based metallic nanowires as bio-nanotransporters. *Nat. Mater.* 3, 692–695. <https://doi.org/10.1038/nmat1205>.
- Peng, P., Guo, W., Zhu, Y., Liu, L., Zou, G., and Zhou, Y.N. (2017). Nanoscale wire bonding of individual Ag nanowires on Au substrate at room temperature. *Nano-Micro Lett.* 9, 26. <https://doi.org/10.1007/s40820-017-0126-8>.
- Peng, Y., Cullis, T., and Inkson, B. (2009). Bottom-up nanoconstruction by the welding of individual metallic nanoobjects using nanoscale solder. *Nano Lett.* 9, 91–96. <https://doi.org/10.1021/nl8025339>.
- Powell, A.W., Stavrinadis, A., de Miguel, I., Konstantatos, G., and Quidant, R. (2018). White and brightly colored 3D printing based on resonant photothermal sensitizers. *Nano Lett.* 18, 6660–6664. <https://doi.org/10.1021/acs.nanolett.8b01164>.
- Powell, A.W., Stavrinadis, A., Christodoulou, S., Quidant, R., and Konstantatos, G. (2020). On-demand activation of photochromic nanoheaters for high color purity 3D printing. *Nano Lett.* 20, 3485–3491. <https://doi.org/10.1021/acs.nanolett.0c00414>.
- Pustovalov, V.K., Smetannikov, A.S., and Zharov, V.P. (2008). Photothermal and accompanied phenomena of selective nanophotothermolysis with gold nanoparticles and laser pulses. *Laser Phys. Lett.* 5, 775–792. <https://doi.org/10.1002/lapl.200810072>.
- Qin, C., Zhang, X., He, W., Zhang, G., Chen, R., Gao, Y., Xiao, L., and Jia, S. (2019). Continuous-wave laser-induced welding and giant photoluminescence enhancement of Au nanospheres. *Opt Express* 27, 2886–2898. <https://doi.org/10.1364/OE.27.002886>.
- Quinten, M., and Kreibig, U. (1986). Optical properties of aggregates of small metal particles. *Surf. Sci.* 172, 557–577. [https://doi.org/10.1016/0039-6028\(86\)90501-7](https://doi.org/10.1016/0039-6028(86)90501-7).
- Rahimi, R., Ochoa, M., and Ziaie, B. (2016). Direct laser writing of porous-carbon/silver nanocomposite for flexible electronics. *ACS Appl. Mater. Interfaces* 8, 16907–16913. <https://doi.org/10.1021/acsami.6b02952>.
- Reguera, J., Langer, J., Jimenez de Aberasturi, D., and Liz-Marzan, L.M. (2017). Anisotropic metal nanoparticles for surface enhanced Raman scattering. *Chem. Soc. Rev.* 46, 3866–3885. <https://doi.org/10.1039/c7cs00158d>.
- Richardson, H.H., Hickman, Z.N., Govorov, A.O., Thomas, A.C., Zhang, W., and Kordesch, M.E. (2006). Thermo-optical properties of gold nanoparticles embedded in ice: characterization of heat generation and melting. *Nano Lett.* 6, 783–788. <https://doi.org/10.1021/nl060105l>.
- Ross, M.B., Blaber, M.G., and Schatz, G.C. (2014). Using nanoscale and mesoscale anisotropy to engineer the optical response of three-dimensional plasmonic metamaterials. *Nat. Commun.* 5, 4090. <https://doi.org/10.1038/ncomms5090>.
- Salmon, A.R., Kleemann, M.E., Huang, J., Deacon, W.M., Carnegie, C., Kamp, M., de Nijs, B., Demetriadou, A., and Baumberg, J.J. (2020). Light-induced coalescence of plasmonic dimers and clusters. *ACS Nano* 14, 4982–4987. <https://doi.org/10.1021/acsnano.0c01213>.
- Sanz, J.M., Ortiz, D., Alcaraz de la Osa, R., Saiz, J.M., González, F., Brown, A.S., Losurdo, M., Everitt, H.O., and Moreno, F. (2013). UV plasmonic behavior of various metal nanoparticles in the near- and far-field regimes: geometry and substrate effects. *J. Phys. Chem. C* 117, 19606–19615. <https://doi.org/10.1021/jp405773p>.
- Seong, B., Chae, I., Lee, H., Nguyen, V.D., and Byun, D. (2015). Spontaneous self-welding of silver nanowire networks. *Phys. Chem. Chem. Phys.* 17, 7629–7633. <https://doi.org/10.1039/c5cp00035a>.
- Sevenler, D., Ünlü, N.L., and Ünlü, M.S. (2015). Nanoparticle biosensing with interferometric reflectance imaging. In *Nanobiosensors and Nanobioanalyses* (Springer), pp. 81–95.
- Shehla, H., Ishaq, A., Khan, Y., Javed, I., Saira, R., Shahzad, N., and Maaza, M. (2016). Ion beam irradiation-induced nano-welding of Ag nanowires. *Micro & Nano Lett.* 11, 34–37. <https://doi.org/10.1049/mnl.2015.0054>.
- Slablab, A., Le Xuan, L., Zielinski, M., de Wilde, Y., Jacques, V., Chauvat, D., and Roch, J.-F. (2012). Second-harmonic generation from coupled plasmon modes in a single dimer of gold nanospheres. *Opt Express* 20, 220–227. <https://doi.org/10.1364/OE.20.000220>.
- Smits, F.M. (1958). Measurement of sheet resistivities with the four-point probe. *Bell Syst. Tech. J.* 37, 711–718. <https://doi.org/10.1002/j.1538-7305.1958.tb03883.x>.
- Sobhani, A., Manjavacas, A., Cao, Y., McClain, M.J., Garcia de Abajo, F.J., Nordlander, P., and Halas, N.J. (2015). Pronounced linewidth narrowing of an aluminum nanoparticle plasmon resonance by interaction with an aluminum metallic film. *Nano Lett.* 15, 6946–6951. <https://doi.org/10.1021/acs.nanolett.5b02883>.
- Solis, D., Jr., Willingham, B., Nauert, S.L., Slaughter, L.S., Olson, J., Swanglap, P., Paul, A., Chang, W.S., and Link, S. (2012). Electromagnetic energy transport in nanoparticle chains via dark plasmon modes. *Nano Lett.* 12, 1349–1353. <https://doi.org/10.1021/nl2039327>.
- Song, T.B., Chen, Y., Chung, C.H., Yang, Y.M., Bob, B., Duan, H.S., Li, G., Tu, K.N., Huang, Y., and Yang, Y. (2014). Nanoscale Joule heating and electromigration enhanced ripening of silver nanowire network transparent electrode. *ACS Nano* 8, 2804–2811. <https://doi.org/10.1021/nn4065567>.
- Spechler, J.A., Nagamatsu, K.A., Sturm, J.C., and Arnold, C.B. (2015). Improved efficiency of hybrid organic photovoltaics by pulsed laser sintering of silver nanowire network transparent electrode. *ACS Appl. Mater. Interfaces* 7, 10556–10562. <https://doi.org/10.1021/acsami.5b02203>.
- Stockman, M.I., Hu, A., Deng, G.L., Courvoisier, S., Reshef, O., Evans, C.C., Mazur, E., and Zhou, Y. (2013). Femtosecond laser induced surface melting and nanojoining for plasmonic circuits. *Proc. SPIE* 8809, 880907. <https://doi.org/10.1117/12.2022482>.
- Su, B., Wu, Y., Tang, Y., Chen, Y., Cheng, W., and Jiang, L. (2013). Free-standing 1D assemblies of plasmonic nanoparticles. *Adv. Mater.* 25, 3968–3972. <https://doi.org/10.1002/adma.201301003>.
- Su, B., Zhang, C., Chen, S., Zhang, X., Chen, L., Wu, Y., Nie, Y., Kan, X., Song, Y., and Jiang, L. (2014). A general strategy for assembling nanoparticles in one dimension. *Adv. Mater.* 26, 2501–2507. <https://doi.org/10.1002/adma.201305249>.
- Sundaraman, R., Narang, P., Jermyn, A.S., Goddard, W.A., 3rd, and Atwater, H.A. (2014). Theoretical predictions for hot-carrier generation from surface plasmon decay. *Nat. Commun.* 5, 5788. <https://doi.org/10.1038/ncomms6788>.
- Taminiau, T.H., Stefani, F.D., Segerink, F.B., and van Hulst, N.F. (2008). Optical antennas direct single-molecule emission. *Nat. Photonics* 2, 234–237. <https://doi.org/10.1038/nphoton.2008.32>.
- Terrones, M., Banhart, F., Grobert, N., Charlier, J.C., Terrones, H., and Ajayan, P.M. (2002). Molecular junctions by joining single-walled carbon nanotubes. *Phys. Rev. Lett.* 89, 075505. <https://doi.org/10.1103/PhysRevLett.89.075505>.
- Tohmyoh, H., Imaizumi, T., Hayashi, H., and Saka, M. (2007). Welding of Pt nanowires by Joule heating. *Scr. Mater.* 57, 953–956. <https://doi.org/10.1016/j.scriptamat.2007.07.018>.
- Van Teijlingen, A., Davis, S.A., and Hall, S.R. (2020). Size-dependent melting point depression of nickel nanoparticles. *Nanoscale Adv.* 2, 2347–2351. <https://doi.org/10.1039/d0na00153h>.
- Wagle, D.V., and Baker, G.A. (2015). Cold welding: a phenomenon for spontaneous self-healing and shape genesis at the nanoscale. *Mater. Horiz.* 2, 157–167. <https://doi.org/10.1039/c4mh00105b>.
- Wang, L., Feng, Y., Wang, K., and Liu, G. (2021). Solar water sterilization enabled by photothermal nanomaterials. *Nano Energy* 87, 106158. <https://doi.org/10.1016/j.nanoen.2021.106158>.
- Wang, Q., Liang, X., Liu, B., Song, Y., Gao, G., and Xu, X. (2020). Thermal conductivity of V2O5 nanowires and their contact thermal conductance. *Nanoscale* 12, 1138–1143. <https://doi.org/10.1039/c9nr08803b>.

- Wang, S., and Ding, T. (2019). Photothermal-assisted optical stretching of gold nanoparticles. *ACS Nano* 13, 32–37. <https://doi.org/10.1021/acsnano.8b06087>.
- Wang, Y., Wang, H., Wang, Y., Shen, Y., Xu, S., and Xu, W. (2016). Plasmon-driven dynamic response of a hierarchically structural silver-decorated nanorod array for sub-10 nm nanogaps. *ACS Appl. Mater. Interfaces* 8, 15623–15629. <https://doi.org/10.1021/acsami.6b04173>.
- Wei, H., and Eilers, H. (2009). From silver nanoparticles to thin films: evolution of microstructure and electrical conduction on glass substrates. *J. Phys. Chem. Solid* 70, 459–465. <https://doi.org/10.1016/j.jpics.2008.11.012>.
- Willems, K.A., and Van Duyn, R.P. (2007). Localized surface plasmon resonance spectroscopy and sensing. *Annu. Rev. Phys. Chem.* 58, 267–297. <https://doi.org/10.1146/annurev.physchem.58.032806.104607>.
- Xi, C., Marina, P.F., Xia, H., and Wang, D. (2015). Directed self-assembly of gold nanoparticles into plasmonic chains. *Soft Matter* 11, 4562–4571. <https://doi.org/10.1039/c5sm00900f>.
- Yamamoto, Y.S., Ozaki, Y., and Itoh, T. (2014). Recent progress and frontiers in the electromagnetic mechanism of surface-enhanced Raman scattering. *J. Photochem. Photobiol. C* 21, 81–104. <https://doi.org/10.1016/j.jphotochemrev.2014.10.001>.
- Yang, C., Wong, C.P., and Yuen, M.M.F. (2013). Printed electrically conductive composites: conductive filler designs and surface engineering. *J. Mater. Chem. C* 1, 4052–4069. <https://doi.org/10.1039/c3tc00572k>.
- Yang, H., Lu, J., Ghosh, P., Chen, Z., Wang, W., Ye, H., Yu, Q., Qiu, M., and Li, Q. (2018). Plasmonic-enhanced targeted nanohealing of metallic nanostructures. *Appl. Phys. Lett.* 112, 071108. <https://doi.org/10.1063/1.5018120>.
- Yao, S., and Zhu, Y. (2014). Wearable multifunctional sensors using printed stretchable conductors made of silver nanowires. *Nanoscale* 6, 2345–2352. <https://doi.org/10.1039/c3nr05496a>.
- Yap, C.Y., Chua, C.K., Dong, Z.L., Liu, Z.H., Zhang, D.Q., Loh, L.E., and Sing, S.L. (2015). Review of selective laser melting: materials and applications. *Appl. Phys. Rev.* 2, 041101. <https://doi.org/10.1063/1.4935926>.
- Yoon, S.S., and Khang, D.Y. (2016). Room-temperature chemical welding and sintering of metallic nanostructures by capillary condensation. *Nano Lett.* 16, 3550–3556. <https://doi.org/10.1021/acs.nanolett.6b00621>.
- Zhang, L., Tang, Y., Peng, Q., Yang, T., Liu, Q., Wang, Y., Li, Y., Du, C., Sun, Y., Cui, L., et al. (2018). Ceramic nanowelding. *Nat. Commun.* 9, 96. <https://doi.org/10.1038/s41467-017-02590-1>.
- Zhang, S.T., Foldyna, M., Roussel, H., Consonni, V., Pernot, E., Schmidt Mende, L., Rapenne, L., Jimenez, C., Deschanvres, J.L., Munozrojas, D., and Bellet, D. (2017). Tuning the properties of F:SnO<sub>2</sub> (FTO) nanocomposites with S:TiO<sub>2</sub> nanoparticles-promising hazy transparent electrodes for photovoltaics applications. *J. Mater. Chem. C* 5, 91–102. <https://doi.org/10.1039/C6TC04153A>.
- Zhou, L., Tan, Y., Wang, J., Xu, W., Yuan, Y., Cai, W., Zhu, S., and Zhu, J. (2016a). 3D self-assembly of aluminium nanoparticles for plasmon-enhanced solar desalination. *Nat. Photonics* 10, 393–398. <https://doi.org/10.1038/nphoton.2016.75>.
- Zhou, W., Bai, S., Ma, Y., Ma, D., Hou, T., Shi, X., and Hu, A. (2016b). Laser-direct writing of silver metal electrodes on transparent flexible substrates with high-bonding strength. *ACS Appl. Mater. Interfaces* 8, 24887–24892. <https://doi.org/10.1021/acsami.6b07696>.
- Zhou, L., Zhuang, S., He, C., Tan, Y., Wang, Z., and Zhu, J. (2017). Self-assembled spectrum selective plasmonic absorbers with tunable bandwidth for solar energy conversion. *Nano Energy* 32, 195–200. <https://doi.org/10.1016/j.nanoen.2016.12.031>.
- Zhou, Y.N. (2008). *Microjoining and Nanojoining* (Elsevier).